CFD Modelling of Weapon Separation from Military Aircraft

By

Muhammad Ali

MS CS&E-12S 00000281832

Supervisor

Dr. Rizwan Riaz

Department of Computational Engineering

School of Interdisciplinary Engineering and Sciences (SINES)

National University of Sciences and Technology (NUST)

Islamabad, Pakistan

November 2022

CFD Modelling of Weapon Separation from Military Aircraft

By

Muhammad Ali

MS CS&E-12S 00000281832

Supervisor

Dr. Rizwan Riaz

A thesis submitted in conformity with the requirements for the degree of *Master of Science* in

Computational Science and Engineering

Department of Computational Engineering

School of Interdisciplinary Engineering and Sciences (SINES)

National University of Sciences and Technology (NUST)

Islamabad, Pakistan

November 2022

Declaration

I, **Muhammad Ali** declare that this thesis titled "**CFD Modelling of Weapon Separation from Military Aircraft**" and the work presented in it are my own and have been generated by me as a result of my own original research.

I confirm that:

1. This work was done wholly or mainly while in candidature for a Master of Science degree at NUST

2. Where any part of this thesis has previously been submitted for a degree or any other qualification at NUST or any other institution, this has been clearly stated

3. Where I have consulted the published work of others, this is always clearly attributed

4. Where I have quoted from the work of others, the source is always given. With the exception of such quotations, this thesis is entirely my own work

5. I have acknowledged all main sources of help

6. Where the thesis is based on work done by myself jointly with others, I have made clear exactly what was done by others and what I have contributed myself

Muhammad Ali

Copyright Notice

To My Family

Acknowledgements

I wish my deepest gratitude to my supervisor **Dr. Rizwan Riaz** for his guidance, advice, criticism, and encouragement throughout the thesis.

I am very thankful to my family for their love, help, and motivation. Without them, this work would not be completed.

I also wish to thank **Dr. Adnan Maqsood** and **Dr. Absar ul Jabar** for their guidance and support during this study. I also would like to thank my colleagues in the Computational Aeronautical lab of NUST for all their help and support during the thesis.

I finally would like to thank anyone who has supported my thesis effort in any way.

Abstract

Fighter aircraft carries various types of stores such as drop tanks, missiles, bombs, and electronic countermeasure components depending on their role and mission requirements. At the time of new aircraft commissioning or major modifications to an older aircraft, the store separation engineer has to gauge the effort toward providing the airworthiness certification for the aircraft and corresponding stores. Typically, engineering analysis, wind tunnel testing, and flight trials are required for this purpose, however, both wind tunnel testing and flight testing are expensive options and carry the risk of human and material loss. As an alternative, computer methods and numerical analysis can now be used instead of flight and wind tunnel tests for certification in some cases. In this study, the store separation process was numerically simulated based on the coupling of Navier-Stokes (N-S) equations with six degrees of freedom (6DOF) rigid-body equations using overset dynamic mesh. The wing-pylon-store configuration (EGLIN test case) at Mach 1.2 was numerically simulated and compared to experimental work to show that the numerical methods can solve the store separation problem. After validation, this thesis addresses the effect of design modification of stores (boat tail and drum-type) and investigates the influence of active and passive flow control devices (Jet and Rectangular blade) on the separation characteristics of a missile from the internal weapons bay. The separation process and flow fields were obtained and all aerodynamic parameters and trajectory parameters were compared. These newly designed control devices can achieve better flow field aerodynamic characteristics, thus increasing missile separation stability. At the leading edge of the cavity, these flow control devices generate shock waves with high pressure, alter the shear layer, and result in a gentle and stable missile attitude. Also, it was found from numerical results modified drum-type weapon raises the shear layer and blocks airflow entering the cavity's back portion. In this case, the shear layer underneath the weapon bay widens, allowing the weapon to travel through it smoothly. The distance between the internal weapons bay and the missile in the positive z-direction with the modification design is 1.6 times that without the modification at t=0.8 s. The pitching angle of the missile ranged from 9° to -9.5°, and the angular motion range of the missile with the modification is smaller than the flow control device cases which indicates optimized modified weapon can get better flow field aerodynamic parameters.

Table of Contents

List of Figures

List of Tables

Chapter 1

Introduction

A critical concern regarding the missile integration process is the safe separation of operational or newly designed missiles from aircraft. Engineering analysis and wind tunnel testing are required. In some circumstances, numerical analysis can substitute flight and wind tunnel experiments. For a safe separation, even validated computational approaches can be employed successfully. As a result, a cost-effective and time-efficient integrating study will conduct. This research aims to analyze the trajectory of stores released from the aircraft's Pylon or cavities and assure their safe release.

1.1. Overview

Checking an aircraft's airworthiness is essential before installing a new store; otherwise, the store could collide with the aircraft's Pylon during its release. There are mainly three approaches to checking the airworthiness and separation trajectories of weapons:

(a) Wind tunnel testing
(b) Flight testing
(c) Numerical approach

Both wind tunnel testing and flight testing are many expensive methods in the above-described methodologies. Moreover, there is always the risk of human and material loss during flight testing. In comparison, the CFD approach to estimating store separation's path is much more cost-effective and freer of danger. In the late 1970s and early 1980s, Computational Aerodynamics finally advanced to the extent of finding a solution for a store in an aircraft flow field. CFD experts hoped to replace the wind tunnel. However, the Wind Tunnel (WT) engineers indicated the CFD community was unaware of the problem's complexity (correctly, since one CFD simulation is unhelpful in estimating a store's trajectory). Flight Test (FT) engineers indicated that neither group could deliver the needed data for a successful program. The relationship between computational fluid dynamics, wind tunnel testing falls under

experimental aerodynamics, and flight testing has been well established and demonstrated in Figure 1.

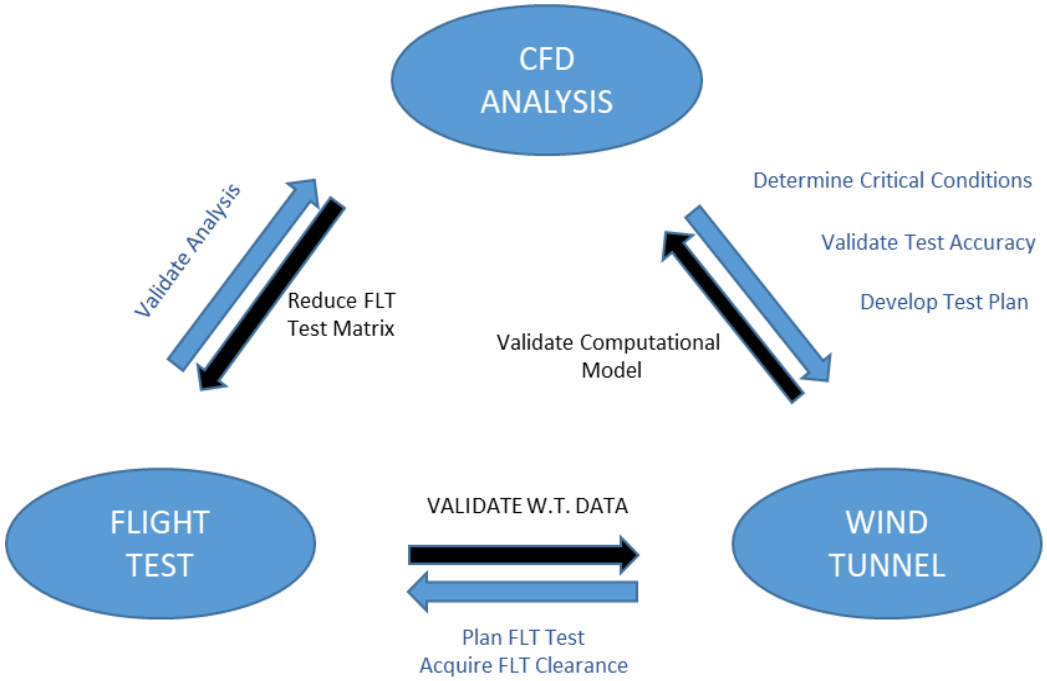

Figure 1: Connection between CFD, Wind Tunnel, and Flight Testing [1]

1.2. Historical Perspective

In the early 20th century, before World War I, military aircraft began to separate their weapons. Even after World War II, the only reason weapons were fallen during testing was to test the store itself or obtain sight settings essential for correct store delivery. Australians launched self-propelled hot air balloons carrying a single bomb against Venice during the First Italian War of Independence in 1849. As a result of World War I, early strategic bombing attempts resulted in the development of specialist bomber aircraft. Initially, bombs were dropped by hand and aimed by the naked eye, as shown in Figure 2.

While jet engines developed quickly after WWII, fighter aircraft could carry sustainable payloads of stores on their wings or fuselage; it became impossible to drop stores and collect ballistic data when the store delivery speed suddenly exceeded Mach-1. It was no longer possible to drop stores and collect ballistic data. The art of separating the store from the aircraft became a problem, requiring careful preflight planning and in-flight prudence. The compatibility of stores with aircraft necessitates engineering assessments and flight testing, including structural, flutter, performance, stability and

control, ballistics, electromagnetic compatibility, and separation. In-flight safety and store separation are by far the most evident of these.

(a)

(b)

Figure 2: Bombs Dropping by Naked Eyes During WWI [2]

1.3. CFD in Aerospace Sector

Using computational mechanics to develop store release configurations and trade studies is now possible. Aerodynamic features for weapon ejection and carriage could be analyzed using Computational Fluid Dynamics. To determine the aerodynamic interference between the aircraft wing and the weapon, CFD is useful. Defining the interference aerodynamics and the surrounding flow field is crucial when analyzing aircraft and store compatibility. CFD has become a critical store clearance tool. CFD will continue to complement experimental approaches such as wind tunnel testing, but it does not expect to replace wind tunnel and flight testing. Some applications like the meshes of the pressure distributions, Velocity stream traces, and the store separation behavior is shown in Figure 3.

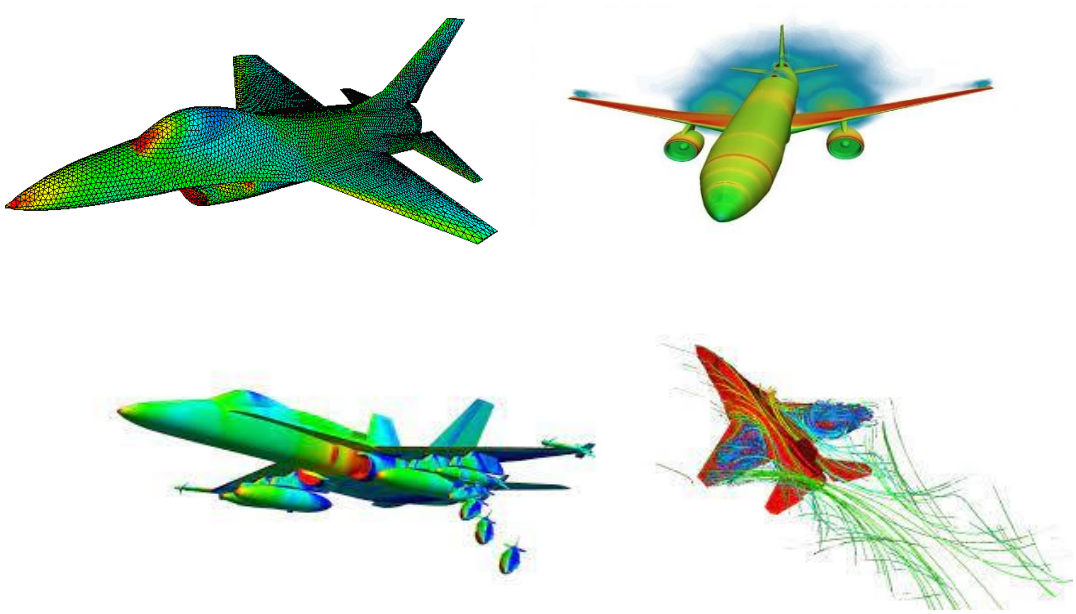

Figure 3: CFD in the Aerospace Sector [3, 4]

1.4. Research Goals and Objectives

- Our first goal is to validate the computational method for weapon separation trajectories against experimental data.
- To understand the store separation flow-field from cavities through CFD simulations.
- To increase the SINES NUST's ability to conduct future research projects involving understanding various stores and missiles with airframes for certification purposes.

1.5. Thesis outline

Chapter 1 of the thesis gives a brief introduction of the store separation process, defines an overview of the history of store separation, also describes the relationship between three approaches, flight test, wind tunnel testing, and CFD approach, used for the certification of a particular weapon introduced in the aircraft industry. This chapter also focuses on research goals and objectives.

Chapter 2 of the thesis focused on a literature review of the CFD methods employed in-store separation. It starts with an overview of the captive trajectory system and then discusses the influence function method and the advancements made over time in-store separation. The core component of this research work is the EGLIN test and the store separations from the internal weapon bays or cavities.

Chapter 3 describes The computational setup employed in this research project. Various stages of computational fluid dynamics (CFD) techniques are discussed, including

modelling of the geometry, generation of the grid, selection of an appropriate turbulence model, the input of the flow parameters, choice of the numerical schemes, convergence criteria, and right time step size for the transient flow analysis.

Chapter 4 focuses on the numerical results of simulations in a very comprehensive manner. In the subsequent chapter, the post-processing Transient analysis results are represented in all pitching, rolling, and yawing directions. In addition, the RANS model has compared these transient numerical results with wind tunnel experimental data. This chapter also gives the effect of variation in-store design modification in decreasing pitch angle. Moreover, this chapter investigates the influence of control devices (JET and RCD) on the store separation characteristics from the cavity.

Chapter 5 summarizes the results of this research and discusses prospectively future directions for this work.

Chapter 2

Literature Review

2.1. Captive Trajectory System

The Captive Trajectory System (CTS) is a technique that has been around since the 1960s [5] and was initially designed for use in wind tunnels for weapon separation. It's an advanced computer-controlled electro-mechanical system with six degrees of freedom (DOF), built for wind tunnel simulation of weapon detachment from a military vehicle. Using CTS, bombs or missiles could be moved along a predicted trajectory while the aerodynamic forces and moments imposed on the payloads are measured and analyzed simultaneously. The Block diagram of a typical captive trajectory system showed in Figure 4.

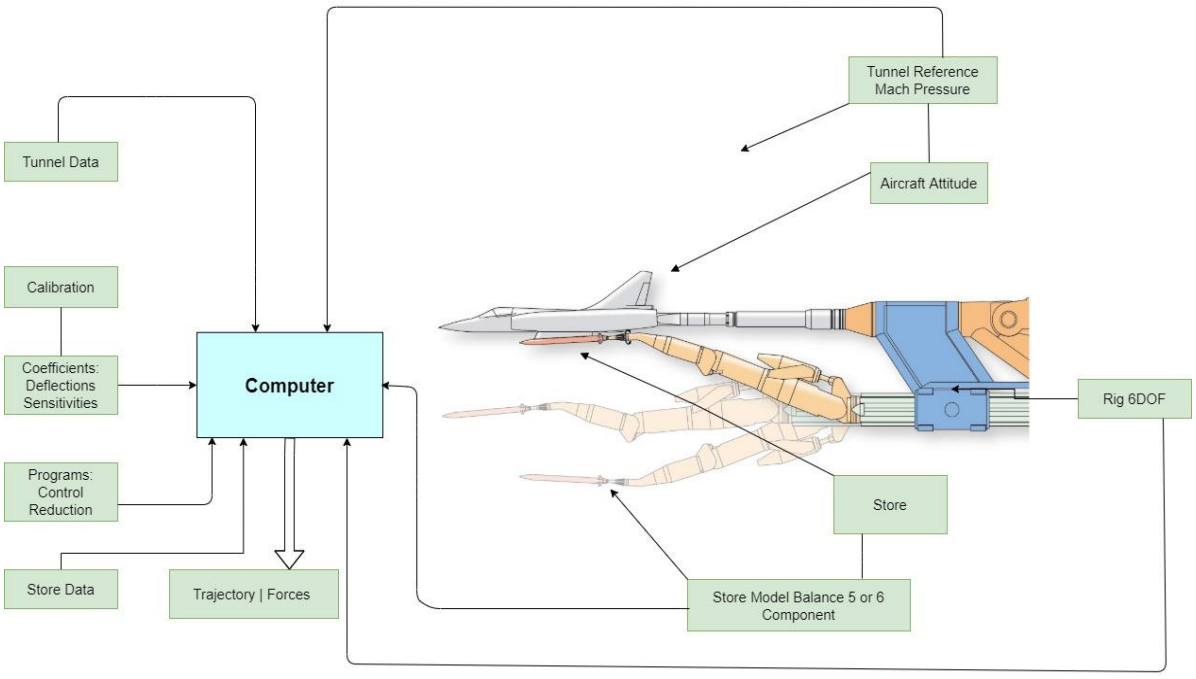

Figure 4: Block diagram of a typical captive trajectory system (CTS) [6]

A Captive Trajectory System (CTS) is a model support system developed specifically for any continuous flow wind tunnel, including Tunnel A, Tunnel B, and Tunnel C. This system has six degrees of freedom (DOF). A pictorial representation of the system's installation is shown in Tunnel A of Figure 5-a. Tunnel A can

accommodate Mach numbers in the range of 1.5 to 5.5, whereas Tunnels B and C of Figure 5-b can accommodate Mach numbers of 6 and 8, respectively. Tunnels B and C feature test sections and model support systems that are virtually indistinguishable from one another.

In 1973, the Arnold Engineering Development Center (AEDC) utilized the von Karman Facility Captive Trajectory System (CTS), which is a computer-controlled method system with six degrees of freedom [7]. This method system was used in Tunnels A, B, and C.

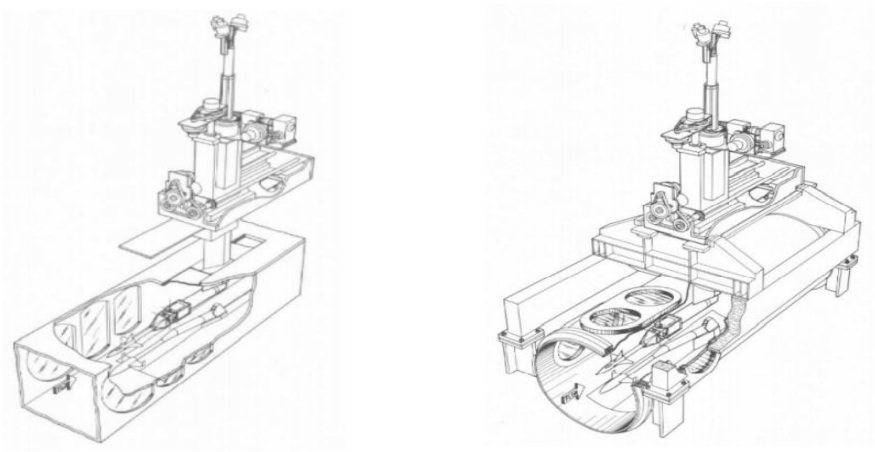

(a) Wind Tunnel A (b) Wind Tunnel B & C

Figure 5: Captive Trajectory System (CTS) [7]

Since then, the Continuous Test Segment (CTS) in Tunnels A and B has conducted various test programs, including the staging and separation of supersonic vehicles. This separation facility complements the Aerodynamic Wind Tunnel's (4T) existing capacity, allowing for conducting subsonic, transonic, and low supersonic research. [8]. When combined, the two methods can perform tests for separating stores at various speeds, from the low subsonic to the hypersonic.

Another approach developed during the 1990's period, called the influence function method (IFM), calculates the store loads based on the flow field in which the store is located [9]. CFD and wind tunnel teams agreed to use this method, as it calculated the entire aircraft flow field of store separation in one calculation.

2.2. Advances in Computational Aerodynamics

2.2.1. During the 1980s

Over the past two decades, the United States Air Force and Navy have collaborated on projects intended to validate and quicken the CFD methodologies used in the store certification process. They accomplished this goal by holding several different conferences. The first one was for the Wing/Pylon/Finned Store at Hilton Head, South Carolina, in the summer of 1992, and it was a massive success. As a result of this initial conference, researchers discovered that full-potential computational methods [9] produced solutions equivalent to those provided by an Euler [10] code for the wing's lower surface when the store was present.

The Office of the Secretary of Defense hosted the second conference held as part of the Applied Computational Fluid Dynamics (ACFD) program at the Department of Defense (OSD). In the summer of 1996, F16 and Generic Finned Store employees gathered in New Orleans. (ACFD Challenge I). The lower-order [11] solutions demonstrated a high level of agreement with the Euler and Navier Stokes codes for this gathering. The F-18/JDAM CFD Challenge was the last conference sponsored by ACFD (ACFD Challenge II). The F/A-18C JDAM configuration had a large amount of wind tunnel and flight test data, Figure 6. Furthermore, all the participants correlated with the wind tunnel and flight test results. The outcomes of the ACFD Challenge II are available in a detailed article [12]. As a result of multiple additional participants joining in the last two years, this setup has become the standard for store separation code validation.

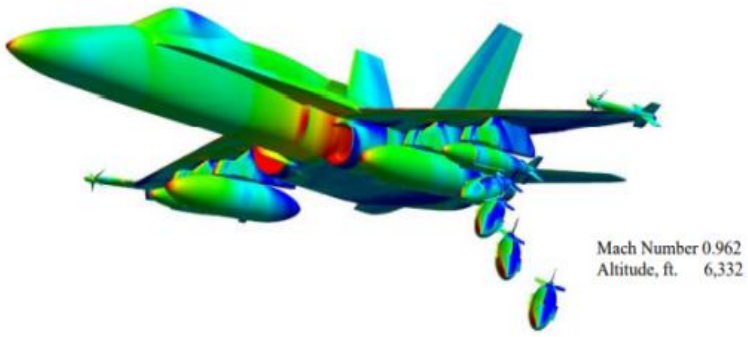

Figure 6: F-18C/GBU-31 Transonic Trajectory Simulation [4]

2.2.2. External Store Separation

The United States Air Force, Army, and Navy each possessed the long-term, proven CFD modelling and simulation capabilities and the software development expertise necessary to enable modern weapon development and integration. Traditional methods of engineering data collection, such as flight and wind tunnel testing, were complemented by each company's use of CFD codes. While working with the High-Performance Computing Center (HPC) in the early 2000s, these three services established the Institute for HPC Applications to Air Armament (IHAAA). Since that time, the application of CFD to store separation analysis has progressed in several ways. As part of the IHAAA initiative, the Air Force provided the Navy with CFD projections, which made it possible to finish the flying clearance process on time. Because of the pressing needs of Operation Iraqi Freedom, the F-18C Canted Vertical Ejector Rack (CVER) located next to the 330-gallon tank needed flight clearance for the GBU-12.

They decided to use a "hit-or-miss" strategy because the Navy did not have a computational model of the GBU-12's store, and the time frame did not allow entry into a wind tunnel test. It was because the time frame did not allow for it. The hit-or-miss method involves letting go of the weapon at an ever-increasing airspeed (by increasing M while remaining at the same height) until it is no longer safe to proceed. Implementing new configurations and expanding the flight envelope for older aircraft is necessary.

Even though the results of the first flight ('M = 0.88, at 5000') were positive, the distance between the first and second store fins and those two fins of the second store and the fuel tank raised concerns about flight safety. As in Figure 7, the outboard store’s open tail and the inboard store’s closed tail are very close. Figure 8 shows the approach of the inboard store tail to the fuel tank, which is a cause for concern.

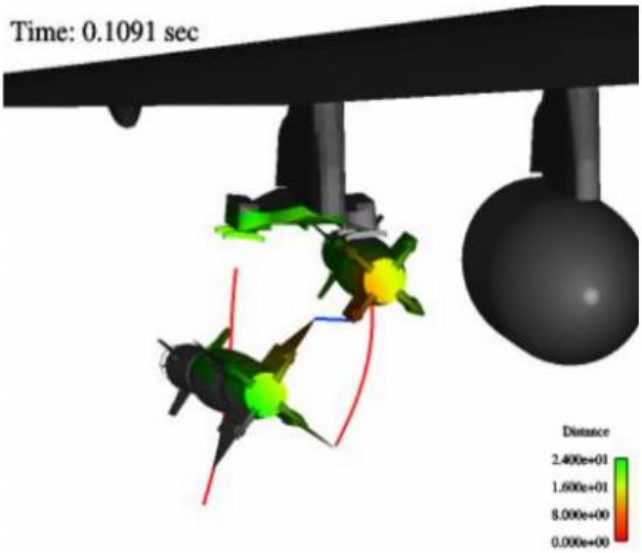

Figure 7: F-18C/GBU-12 Outboard [4]

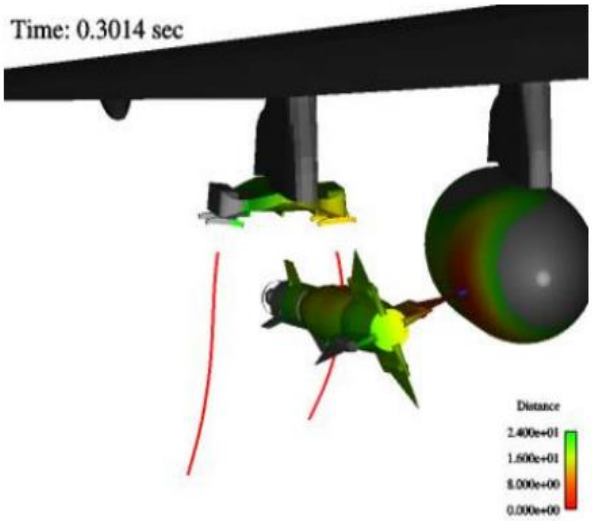

Figure 8: F-18C/GBU-12 Inboard [4]

In most cases, the Navy will not go any further if the missing distance is less than six inches unless the wind tunnel indicates it is safe. Fortuitously, the Air Force SEEK EAGLE office had the F-18C/D geometry because they had participated in the ACFD trajectory calculations [13] performed for the GBU-12 store and offered to do the CFD calculations simultaneously with the flight testing program. These calculations had to be done to ensure that the F-18C/D could fly safely. In addition, their predictions were in perfect agreement with flight test data, resulting in a successful flight test

program. More information about this and other IHAAA research can be found here [10, 14, 15].

2.2.3. Internal bay weapon separation

The utilization of an internal weapons bay in combat aircraft can help to reduce aerodynamic drag, aerodynamic heating, and radar signature [16, 17]; Nevertheless, it also causes a large number of complex flow phenomena [18-20] and increases the risk of missile separation from the weapons bay. Therefore, it is of the utmost importance to investigate the procedure for separating a missile's internal weapons bay and the flow control mechanism. The flows that occur around an internal weapons bay are typical examples of cavity flows. Since the 1950s, when aircraft got internal weapons bays, scientists have been curious about cavity flow. Over the last few years, much academic interest has been in controlling cavity flow [18, 19, 21-25]. Flow control is classified into two types: active and passive.

When using passive control, there is no input of external energy into the flow, and the flow field is typically controlled by modifying the geometric shapes of the environment, such as by adding spoilers, ramps, and other features [10, 26]. On the other hand, active control systems involve external energy input in jets or oscillating flaps [18, 27].

Releasing a bomb from the cavity is hazardous and requires extensive research. Stallings performed a store separation experiment at Mach 2.36 in the Langley Unitary Plan Wind Tunnel [16] to estimate the near-field separation parameters of a standard wing-control missile design from a cavity of varying depths. Davis *et al*. [28] analyzed how sensitive the trajectories are to the various store separation settings. The examination of high-speed store delivery from the cavity was carried out by Xue *et al*. [29] in a sub-transonic and supersonic wind tunnel measuring 0.6 meters by 0.6 meters.

When a store is removed from an inside weapons bay, there is a possibility that it will come back under certain flight conditions [30-32]. To overcome this issue, researchers working on the HIFEX Program [33], which DARPA sponsored, developed an active control mechanism. This mechanism guarantees the safe discharge of a thin axisymmetric store from a rectangular cavity under an external supersonic flow. Sahoo *et al*. [32] constructed a low-order model that integrates the primary elements that drive the store trajectories with and without micro jet and delineates safe and unsafe departure

circumstances. This model was published in Science Advances. Finally, bower *et al*. [33] created a system of active flow control that can be used to deploy high-speed weapons from a cavity

Chapter 3

Problem Formulation and Computational Framework

3.1. Introduction

It is a numerical technique that calculates and predicts the fluid flow as it interacts with an object of interest, a process known as computational fluid dynamics. Besides fluid flow, it can also examine chemical processes, heat and mass transport, and their combined behaviours. Experimentation and analytical techniques understand fluid flow behaviour but provide limited insight into the details due to their inability to a range of information on different flow parameters and have limited capacity to solve complex flows compared with computational fluid dynamics. CFD technique uses numerically calculating the governing partial differential equations at every point on the grid, a process known as grid computing. These points could be on the mesh's nodes (ANSYS ® CFX) or cell centres (ANSYS ® FLUENT).

Aside from that, CFD is now frequently employed because it is less expensive than traditional experimental procedures (wind tunnel, water tunnel). In addition, analytical techniques are either developed for simplified examples or are too sophisticated to predict the flow phenomena of real-world problems.

CFD is not a replacement for any of these approaches. However, each of them has its value and application. For example, Navier-Stokes equations are complex, nonlinear partial differential equations that can be solved using the discretized algebraic form in computational fluid dynamics or CFD.

3.2. Reynolds Averaged Navier-Stokes (RANS) Equations

In turbulent flow, the molecules move chaotically along complex irregular paths. This strong irregular motion intensely causes the various layers of the fluid to mix. If velocity is an instantaneous quantity, it decomposes into two parts, the ensemble-averaged component ū and the fluctuating component u'.

$$u = \bar{u} + u' \tag{3.1}$$

And,

$$\bar{u} = \frac{1}{T_1}\int_t^{t+T_1} u_i(x,t)dt \tag{3.2}$$

Where is it long enough to include sufficient fluctuations to give a stable value? The following Figure 9 illustrates the Time-averaging of non-stationary turbulence.

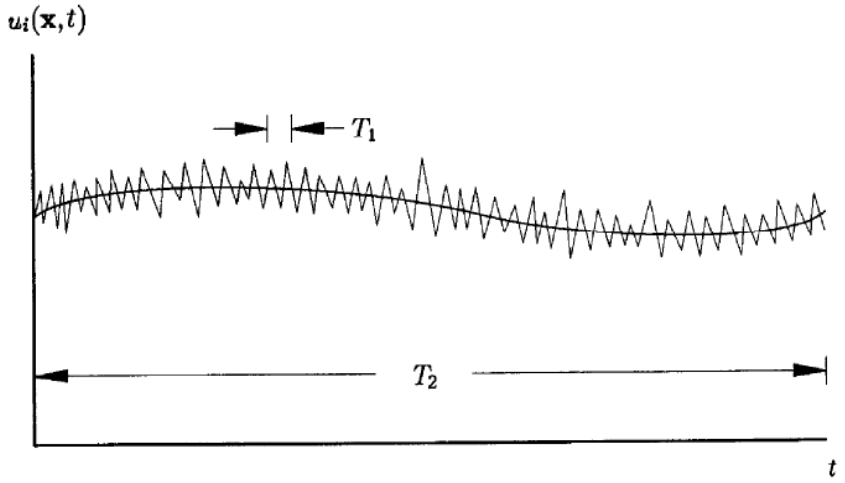

Figure 9: Time Averaging for Non-Stationary Turbulence

The momentum equation for the ith component of velocity vector reads as

$$\frac{\partial(\rho u_i)}{\partial t} + \frac{\partial(\rho u_i u_j)}{\partial x_j} = -\frac{\partial p}{\partial x_i} + \frac{\partial}{\partial x_j}\left[\mu\left\{\frac{\partial u_i}{\partial x_j} + \frac{\partial u_j}{\partial x_i}\right\}\right] \tag{3.3}$$

Where ρ is density and μ is the viscosity. By breaking the variables of this equation into average and fluctuating parts and then applying ensemble averaging, we get the equation of the form:

$$\frac{\partial(\rho \bar{u}_i)}{\partial t} + \frac{\partial(\rho \bar{u}_i \bar{u}_j)}{\partial x_j} = -\frac{\partial \bar{p}}{\partial x_i} + \frac{\partial}{\partial x_j}\left[\mu\left\{\frac{\partial \bar{u}_i}{\partial x_j} + \frac{\partial \bar{u}_j}{\partial x_i}\right\}\right] - \rho\frac{\partial(u_i' u_j')}{\partial x_j} \tag{3.4}$$

This new equation has an additional unknown term when written in tensor form. For a three-dimensional case, this tensor term expands into nine new terms, which reduce to six because of symmetry. These unknown terms are called Reynolds stress terms. The total stress reads as follows:

$$\tau_{ij} = \mu\left\{\frac{\partial \bar{u}_i}{\partial x_j} + \frac{\partial \bar{u}_j}{\partial x_i}\right\} - \rho(\overline{u_i' u_j'}) \tag{3.5}$$

The first term on the right side of the equation is laminar stresses, and the second term is known as turbulent stresses. To calculate turbulent kinetic energy, we add the Reynolds stresses together, as shown below:

$$K_t = \frac{1}{2}\left(\overline{u'u'} + \overline{v'v'} + \overline{w'w'}\right) \tag{3.6}$$

The turbulence intensity, on the other hand, is the root mean square value of fluctuating velocities, referred to as characteristic mean flow velocity, namely *Uo*:

$$I_x = \left(\frac{\sqrt{\overline{u'u'}}}{U_o}\right), I_y = \left(\frac{\sqrt{\overline{v'v'}}}{U_o}\right), I_z = \left(\frac{\sqrt{\overline{w'w'}}}{U_o}\right) \tag{3.7}$$

The steady-state case simulation uses non-moving frames. For this, the conservation of mass is given by,

$$\frac{\partial \rho}{\partial t} + \frac{\partial}{\partial x_j}(\rho u_j) = 0 \tag{3.8}$$

Where uj is averaged mass velocity in the jth direction. Similarly, the conservation of momentum equation is given by,

$$\frac{\partial}{\partial t}(\rho u_i) = +\frac{\partial}{\partial x_j}(\rho u_i u_j) = \frac{\partial}{\partial x_j}\left[-\left(p + \tfrac{2}{3}\rho k\right)\delta_{ij} + \tau_{ij}\right] \tag{3.9}$$

Where k is the turbulent kinetic energy, p is the pressure. The conservation of total energy per volume is,

$$\frac{\partial E_t}{\partial t} + \frac{\partial}{\partial x_j}([E_t + p]u_j) = \frac{\partial q_j}{\partial x_j} + \frac{\partial}{\partial x_i}(u_j \tau_{ij}) - \frac{\partial}{\partial x_j}\left(\sum_{s=1}^{ns} h_s J_{s,j}\right) \tag{3.10}$$

Where q_j is the heat flux in the j^{th} direction.

3.2.1. Flow Field Conservation Equations for Moving Volumes

These equations use for the moving volumes, i.e., release simulation of the store for the safe trajectory. For a general function, the relationship between the time rate change of a function integrated over a volume, the volume integration of a time derivative, and the effect of moving volume surfaces is given by,

$$\frac{d}{dt}\int_V f dV = \int_V \frac{df}{dt} dV + \int_S \vec{v}_g . \hat{n} f dS \tag{3.11}$$

Where in this function, V is the volume, t is the time, and vg is the volume surface. Relating this theorem to previous conservation equations, the conservation of mass is used as an example. First, the partial differential equation integrates over a volume.

$$\int_V \frac{\partial \rho}{\partial t} dV + \int_V \nabla.(\rho \vec{v}) dV = 0 \tag{3.12}$$

Using the Divergence Theorem gives,

$$\frac{d}{dt}\int_V \rho dV + \int_S \rho\left(\vec{v} - \vec{v}_g\right).\hat{n} dS = 0 \tag{3.13}$$

Similarly, all conservation equations can be manipulated such that,

$$\frac{d}{dt}\int_V Q dV + \int_S (\vec{F}_c - Q\vec{v}_g - \vec{F}_D).\hat{n} dS = \int \Omega \, dV \tag{3.14}$$

Q is the conserved variable vector, F_c is the convective (inviscid) flux, F_d is diffusive (viscous) flux, v_g is the volume surface velocity, and **Ω** is the source terms.

3.3. Computational Setup

An essential subfield of computational science is known as computational fluid dynamics (CFD), and it describes the process of employing computers to find solutions to issues about fluid mechanics. For example, CFD software performs calculations of the Navier-Stokes Equations at various grid positions using multiple numerical methods and schemes. Every CFD problem follows the same workflow, breaking into three primary stages.

3.3.1. Pre-processing

Pre-processing in the CFD software workflow involves preparing geometry, meshing the geometry, and setting up the material properties and initial and boundary conditions.

3.3.2. Processing

The next step is to specify the numerical parameters, which include things like the solver specifications and the methods of discretization, among other things. Each

project has a unique design, depending on the simulation used. Numerous solvers can solve a problem with varying values for the solver parameters; however, it is essential to provide the appropriate values for the solver specifications and numerical techniques to solve the problem most effectively.

3.3.3. Post-processing

Analyzing a numerical simulation is one of the most crucial aspects of the process and is done in the post-processing stage of the project. Different filters, such as streamlines, and contour plots, are used to study the flow fields. Post-processing is an integral part of the CFD workflow and allows you to visualize the results of your simulations and the various design optimization tools. In addition to tables, graph plots, and colourful contour drawings (contour maps), these data can even be present in the form of flow animations [34]. Steps followed for solving a physical problem with CFD are presented in Flow Chart (Figure 10).

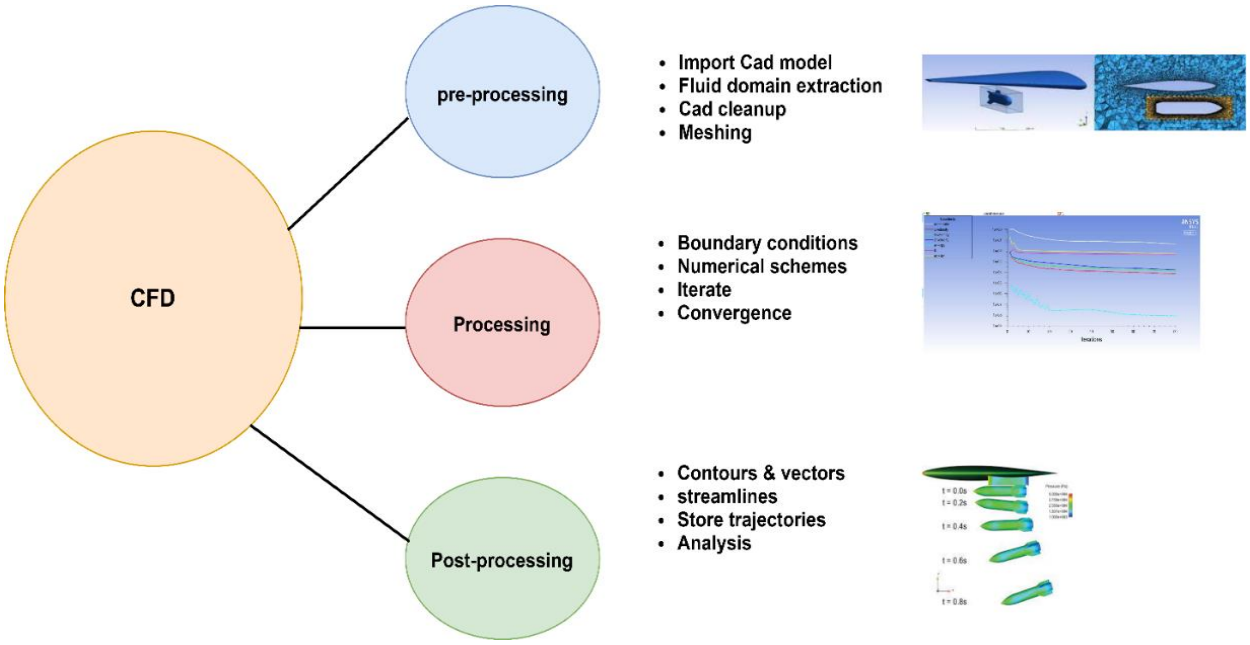

Figure 10: Flow chart of physical problem using CFD

3.4. Geometry Configuration

3.4.1. Wing geometry

The wing profile consists of the NACA 64A010 airfoil section, which has a constant pattern across the wing. The leading edge has a 45-degree sweep angle, whereas the trailing edge has no sweep. The wing's root and tip chords measure 15 and 2 inches, respectively. The wing's half span is 13 inches, while the taper ratio is 0.133.

3.4.2. Pylon geometry

There are two types of the cross-section for the configuration: ogive-flat plate-ogive shape and tangent-ogive shape. The Pylon is 0.294 inches wide and 4.5 inches in length. At both ends, the ogive section's radius is 1.25 inches while its length is 0.5 inches. Figure 11 shows a detailed representation of the Pylon.

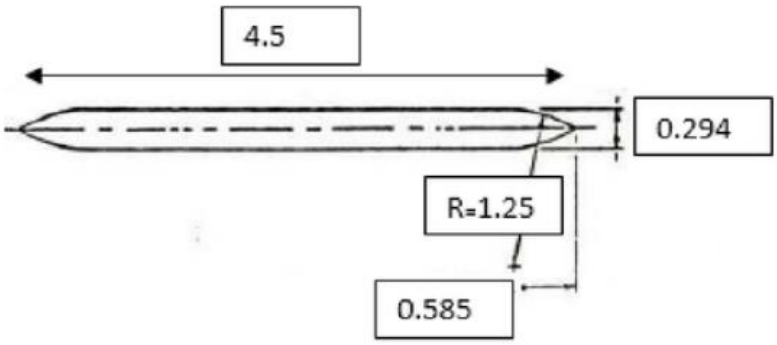

Figure 11: Pylon geometry [35]

3.4.3. Store geometry

The store model shape is composed of a tangent-ogive fore body and after body. The diameter of the store is 1 inch, which contains four fins arranged in a cruciform around the tail region. These fins are identical and have a constant airfoil shape NACA OOO8, with the root and tip chord lengths of 1.667 and 1.061 inches, respectively. Likewise, the store has a leading-edge sweep angle of 60 degrees. As a result, the store locates 0.070 inches away from the Pylon. Moreover, the store nose is about 1.667 inches ahead of the Pylon. Figure 12 shows the store model's detailed drawings.

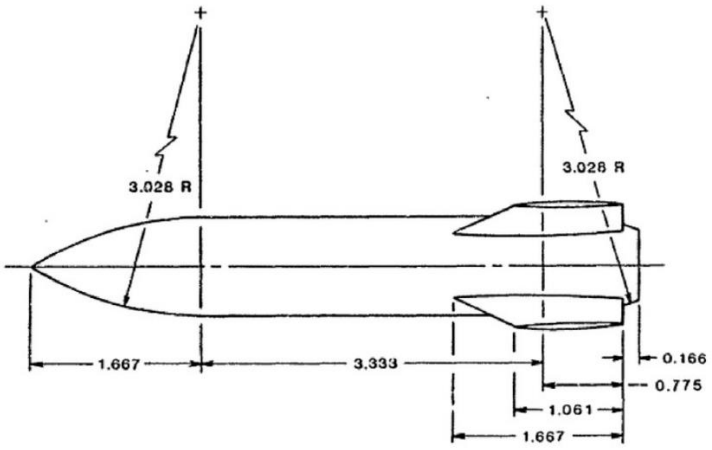

Figure 12: Store geometry [35]

3.4.4. Modified store geometry reconstruction

A boat tail is a name given to the tapered section of the body at the rear. The boat tail is there to reduce the drag caused by a body with a squared-off base. Figure 13-a shows how "boat-tailing" the back reduces the base area. Figure 13-b and 13-c show the side and back view of a generic store's "drum type" model. The tail is a cylindrical shroud ring supported from the after body on four symmetrical fins.

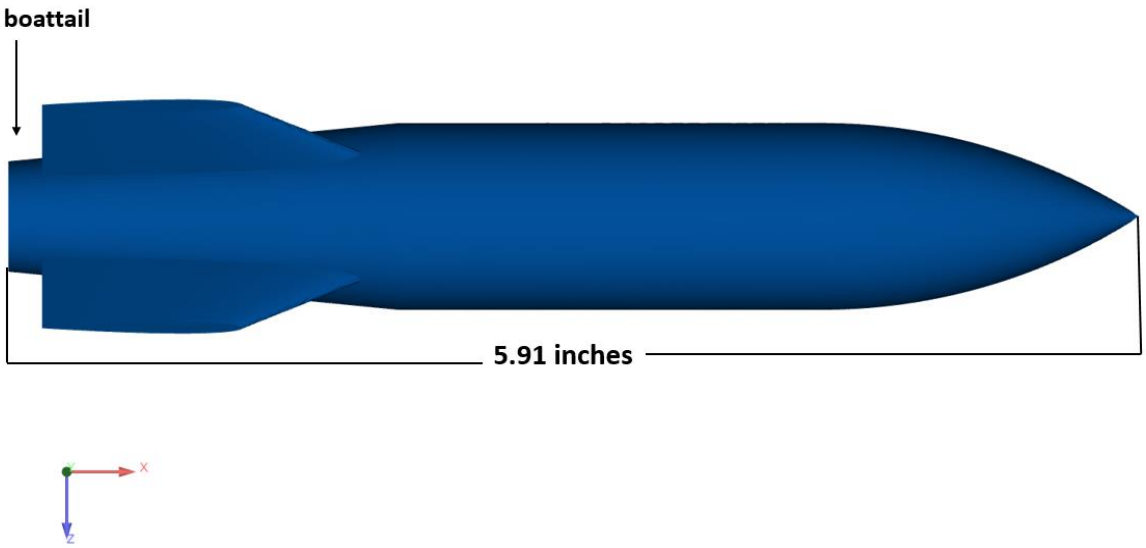

(a) Modified store

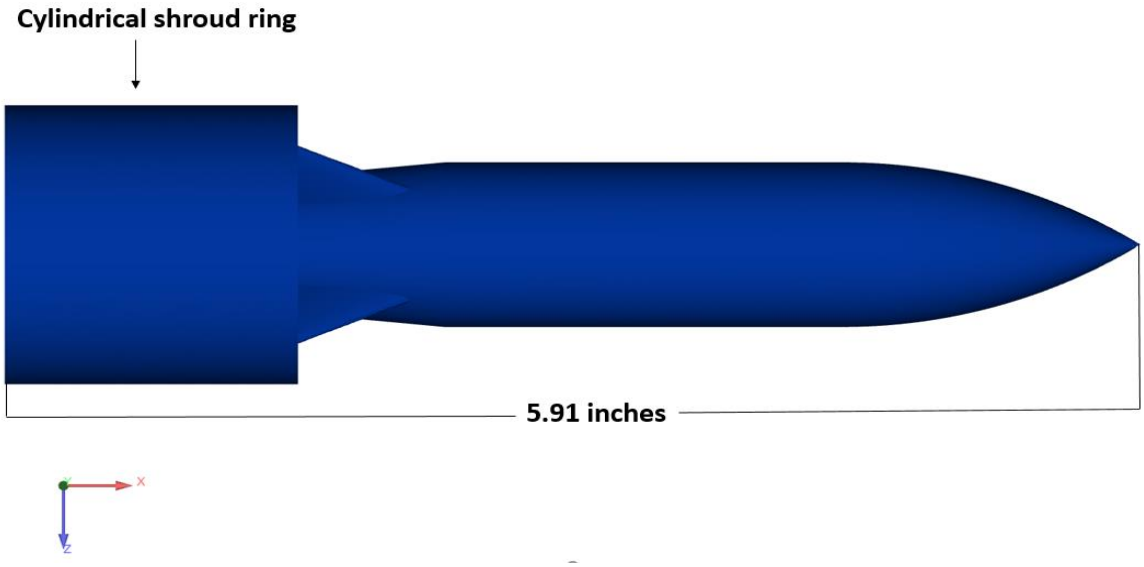

(b) Drum-type store

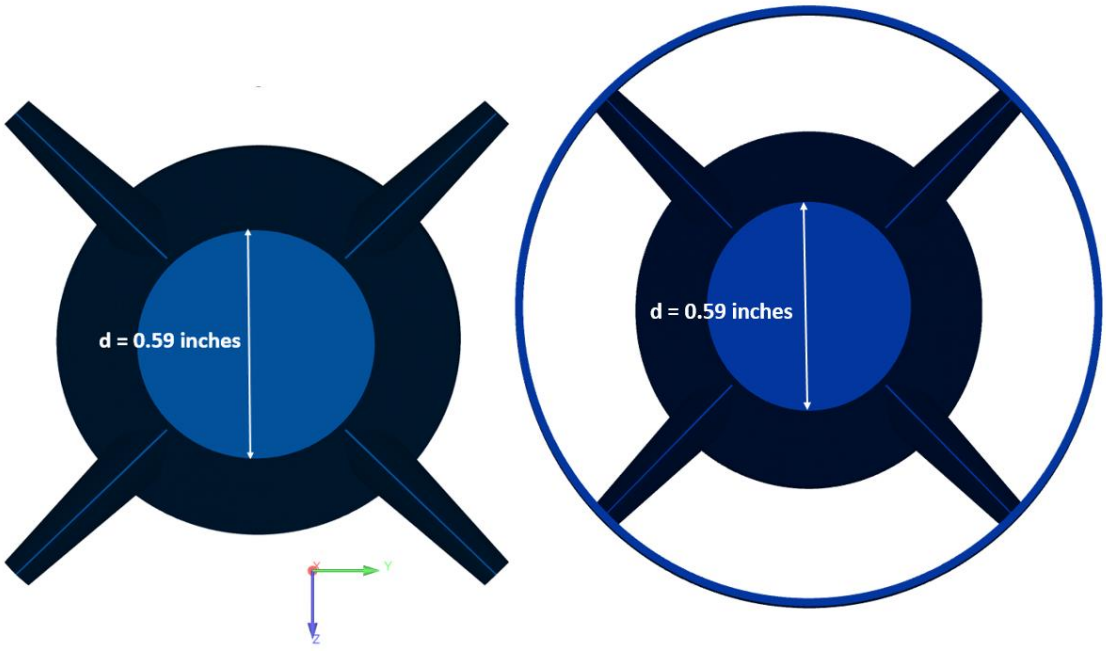

(c) back view

Figure 13: Modified store geometry reconstruction

3.5. Computational Domain

3.5.1. Eglin Case

The computational domain extends to about 16 times wing length in all directions around the geometry. Figure 14 depicts the boundary conditions. Downstream, upstream, and all-side boundaries were Far-Field (characteristics-based inflow/outflow), with the right-side assumed symmetric.

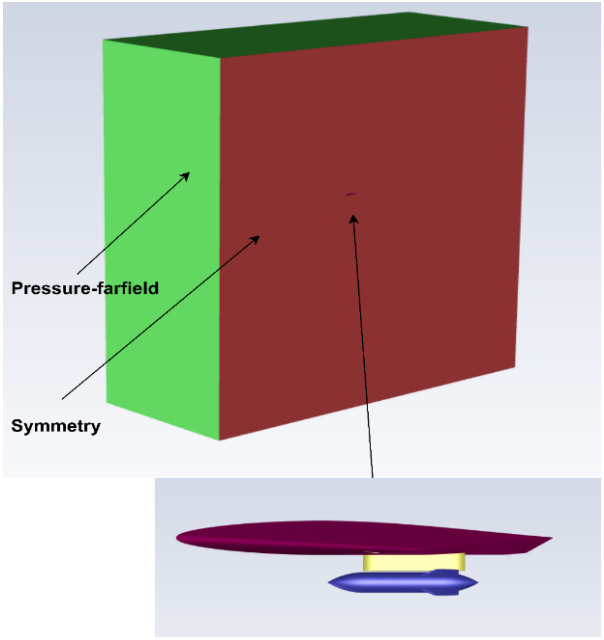

Figure 14: Solution domain

3.5.2. Cavity case

Figure 15 depicts the boundary conditions and computational domain. The missile and bay boundary conditions were no-slip wall conditions, while the pressure far-field boundary conditions were selected as other boundaries. Pressure far-field conditions are used in ANSYS ® FLUENT to model a free-stream state at infinity, with a free-stream Mach number and static conditions being specified.

The internal weapon cavity was rectangular with dimensions of L×W×B = 7.8inches×2inches×2.3inches. The dimensions of the rectangular control device (RCD) were Δx = 0.3 inches, Δy = 2.3 inches, and Δz = 0.48 inches. The diameter of the jet was $\mathbf{d_3}$ = 0.09 inches, its distance from the front border of the cavity to its center was $\mathbf{d_1}$ = 0.18 inches and its distance from the other jet was $\mathbf{d_2}$ = 0.15 inches.

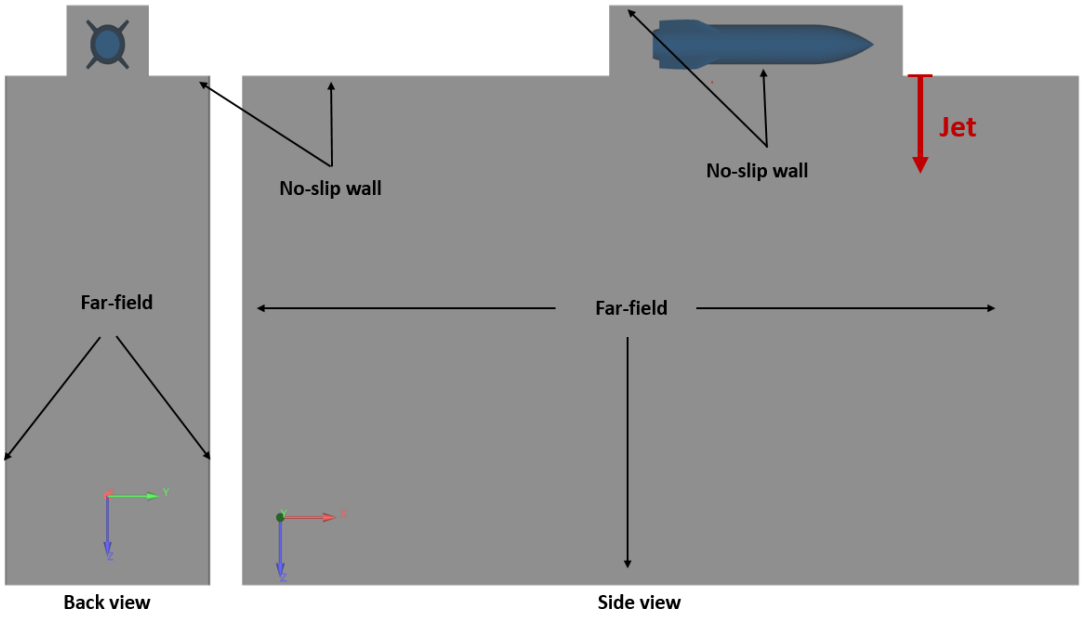
No-slip wall
No-slip wall
Jet
Far-field
Far-field
Back view
Side view

(a)

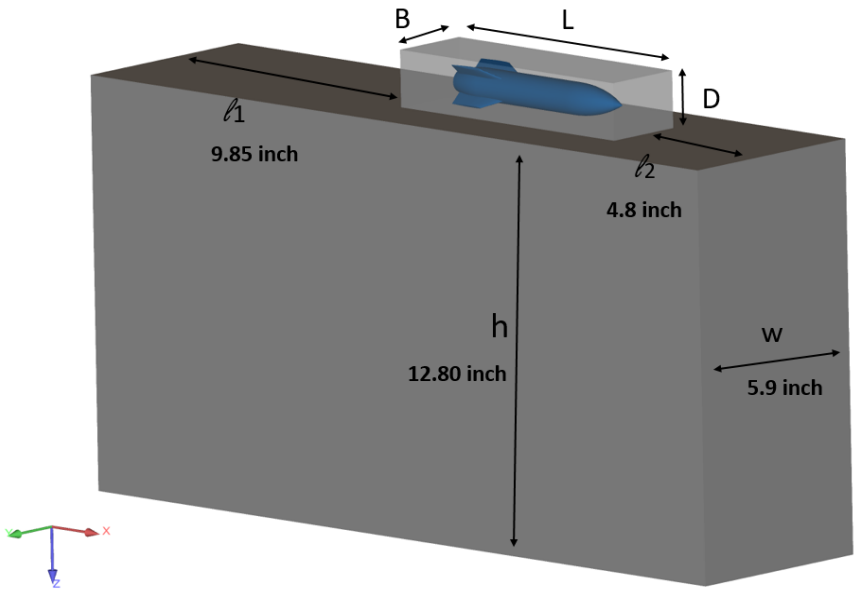
B
L
D
ℓ_1
9.85 inch
ℓ_2
4.8 inch
h
12.80 inch
w
5.9 inch

(b)

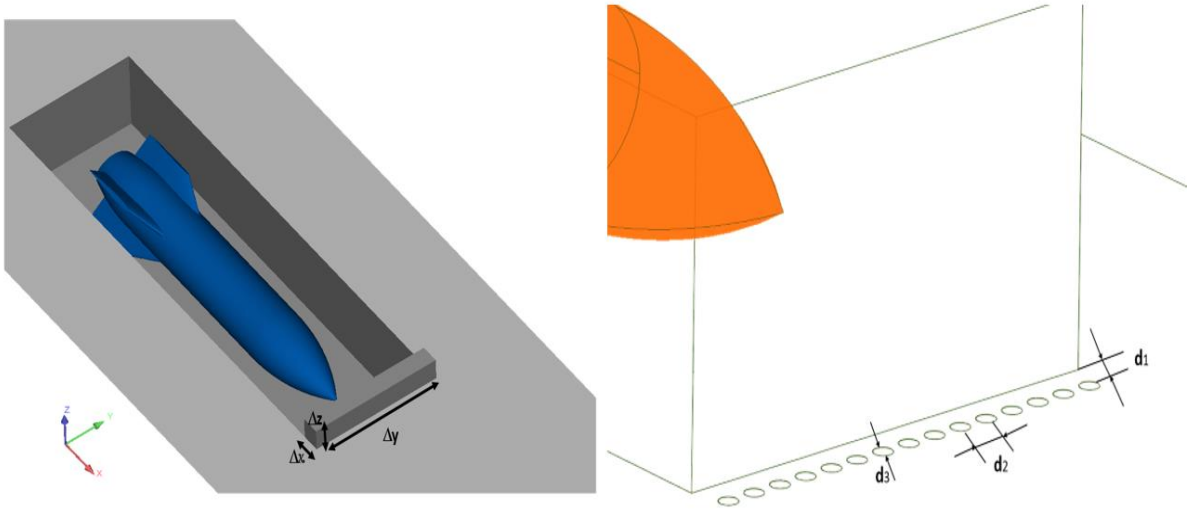

(c)

Figure 15: Computational domain and boundary conditions

3.6. Computational Mesh

Grid/mesh generation is the process of dividing the interest domain into several small parts or subdomains. Creating a grid, also known as meshing, is a crucial step in the CFD simulation process because it is essential to getting accurate CFD results. The skill level and kind of mesh used also impact simulation time, stability, and solution convergence. The most time-consuming step in a CFD analysis is typically meshing generation.

ANSYS ® MESHER is used to generate the unstructured computational grid for CFD analysis. The grid is densely clustered near the body surface to precisely resolve intricate flow features. Face sizing is used on store, pylon, and wing surfaces to get a good grid resolution for displaying the surface geometry.

An internal block was built within the Fairfield domain to reduce the occurrence of overset dead cells in the ANSYS ® FLUENT solver. The store moves only in this region. The boundary condition of the block is selected as an interior. In the overset dynamic mesh approach, we define two mesh zones overlapping. Zone 1 comprises Farfield and interior block, whereas zone 2, meshed separately, consists of overset domain around the store body.

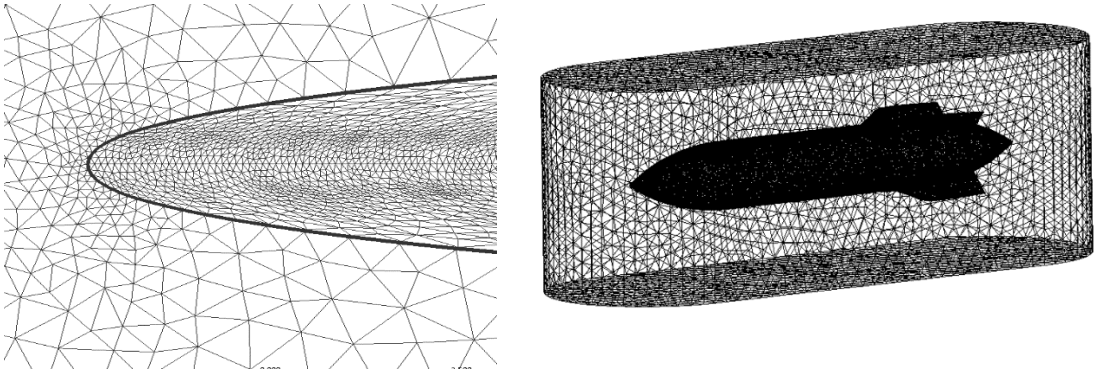

(a) **(b)**

Figure 16: Mesh around wing and store

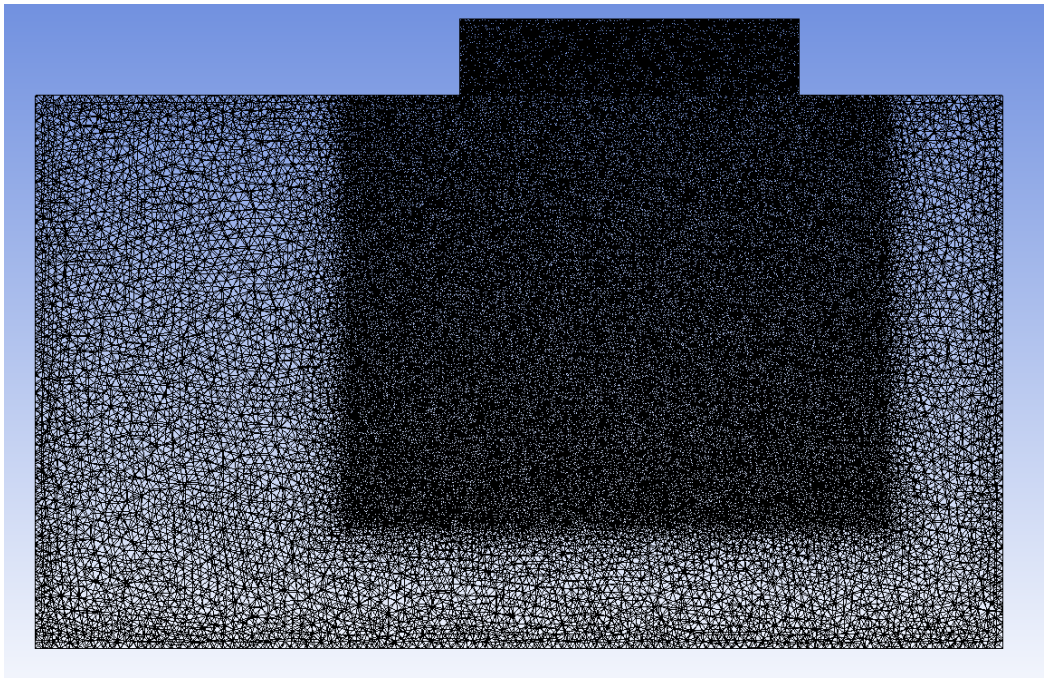

Figure 17: Mesh distribution in cavity case

3.7. Chimera/Overset Grid Methodology

3.7.1. Introduction

In the domain of fluid dynamics, an invention known as the overset approach has just emerged (CFD). It has been employed in computational fluid dynamics (CFD) for over twenty years and has successfully dealt with complicated geometries. The overset technique prevents the need for grid re-meshing whenever it applies to applications with dynamic boundary flow. Recently, unstructured grids have been used in the overset grid system to make it easier to create grids for each sub-domain [36].

This approach also prevents repeated meshing of the whole geometry and enables the straightforward replacement and duplicate of a specific portion.

In the overset method, two or even more cell zones are allowed to overlap with one another. One cell zone is kept motionless and is referred to as the background, whereas the other cell regions are elements that can experience rigid body motions. The background cell zone is the only zone that does not move during the procedure.

The hole-cutting method [37], which deactivates multiple cells in overlapping zones, is followed by the adaptive creation of an interface between the cell zones to give a continuous solution. Dead cells are cells that have lost their ability to function normally. Donor cells are those cells within a cell zone that can communicate information to other cell zones that overlap. On the other side, receptors are cells responsible for collecting data from donors. Figure 18 provides a schematic representation of an overlapping component and a background zone.

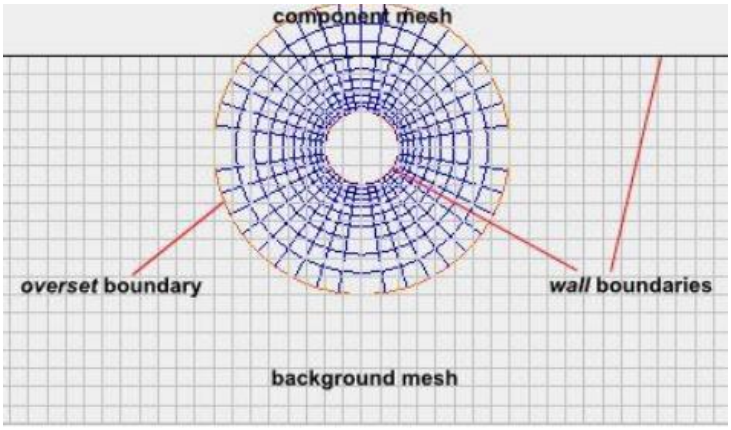

Figure 18: Schematic drawing of overlapping component and background zones [38]

3.7.2. Overset Interpolation

In the overset method, receptor cells located close to the interface between the two sets of data receive information from many donors, as follows:

$$\emptyset^{h} = \sum_{i=0}^{Nd} w^{i}\phi^{i} \qquad (1)$$

Where w represents the interpolation weights, stands for the solution variable, and is the total number of donors.

The overlaying of a rectangular Grid-2 receptor cell with a triangle-shaped Grid-1 cell shows in Figure 19. Face or node connection determines the number of donors for every receptor in the core donor's neighbourhood. The donor cell in a receptor's overlapping cell zone is its leading donor. Face-connected donors are cells that connect faces with a primary donor, and solid lines depict their connections to that primary donor. Cells that donate to a primary donor and share nodes are called node-connected donors.

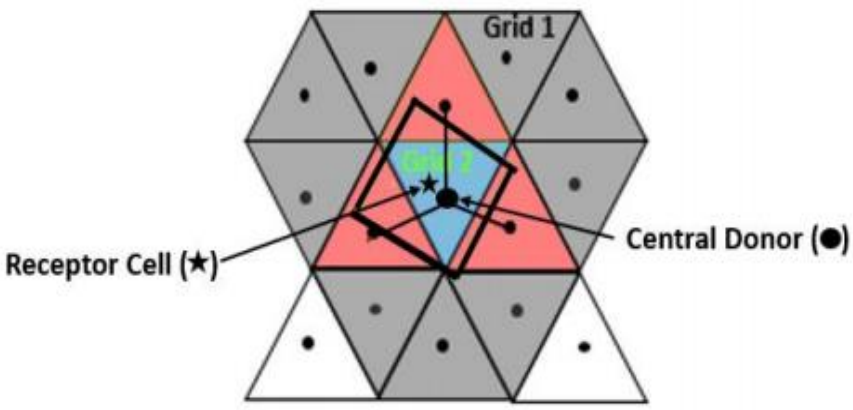

Figure 19: Overlapping component, background grids, and nearby donors of a receptor cell [39]

The overset method computes interpolation weights based on receptor and donor relationships. The interpolation approach updates the information of the receptor cell, and then reconstructions and viscous gradients are calculated. A linear system connects cells of the same or separate grids. Parallel solvers solve the resulting inter-grid linear system. After solving the linear system, related donors' receptor cell information is updated. Standard discretization processes allowed the receptor cell and its neighbours on the same grid to edit data on receptor cell faces.

Although the Overset method is not typically considered conservative, it is possible to significantly cut down on the number of conservation errors by ensuring that the cell size ratio between the receptor and donors remains within a range that is considered reasonable. In an ideal situation, the ratio would be 1:1. Dealing with orphan cells, which are receptors that do not have proper donors, is one of the key obstacles to be overcome to generate an overset mesh. Orphan cells can cause numerical solutions to become unstable, leading to results that are not physically possible. ANSYS ® FLUENT includes a numerical treatment that can automatically update orphan cells

depending on the data from their neighbouring cells. This treatment is active by default. On the other hand, it possesses a mesh resolution that is high enough to prevent the generation of orphan cells [40].

3.8. Boundary Conditions

The purpose of this present study is to investigate store separation for the supersonic (Ma=1.2) domain. Downstream, upstream, and all side borders other than the right-side boundary are defined as pressure far-field, whereas the right-side limit is symmetry.

A second-order precise, upwind extrapolation is employed to determine the flow variables' values at the boundary. The k-epsilon model, mainly designed for aerospace applications with wall-bounded flows, has shown outstanding performance for boundary layer thickness subject to adverse pressure gradients. Therefore, the K-epsilon two-equation wall treatment model was used to model the turbulence, and it is suitable for y + =1 with the ideal gas equation. Below are free stream flow properties (Table 1).

Table 1: Free Stream Flow Quantities [39]

Flow Speed, Mach no.	1.2
Altitude, m	11600
Pressure, Pa	20589
Temperature, K	216.6
Density, kg/m3	0.5298364
Velocity, m/s	353.94
Viscosity, Pa.s	3.5718 x 10−5
Acceleration due to gravity, m /s2	9.81

3.9. Numerical Methodology

In this research study, the modelled store configuration includes not one but two ejection points. The Naiver-Stokes flow solver couples with six Degree of Freedom (DOF) equations with a density-based finite-volume solver for compressible flow. The predicted calculated trajectories validate with the experimental data obtained from a 1/20 scale wind tunnel test at the Arnold Engineering Development Center (AEDC) [7].

The CFD analysis results, such as the position of the centre of gravity, the orientation of the centre of gravity, and the linear and angular speeds, are validated by comparing them to experimental data published in the relevant academic literature. After validation, this research studies analyze the Simulation of the Store Separation from Internal Weapons Bays. Figure 20 shows the numerical methodology in the form of a flow chart.

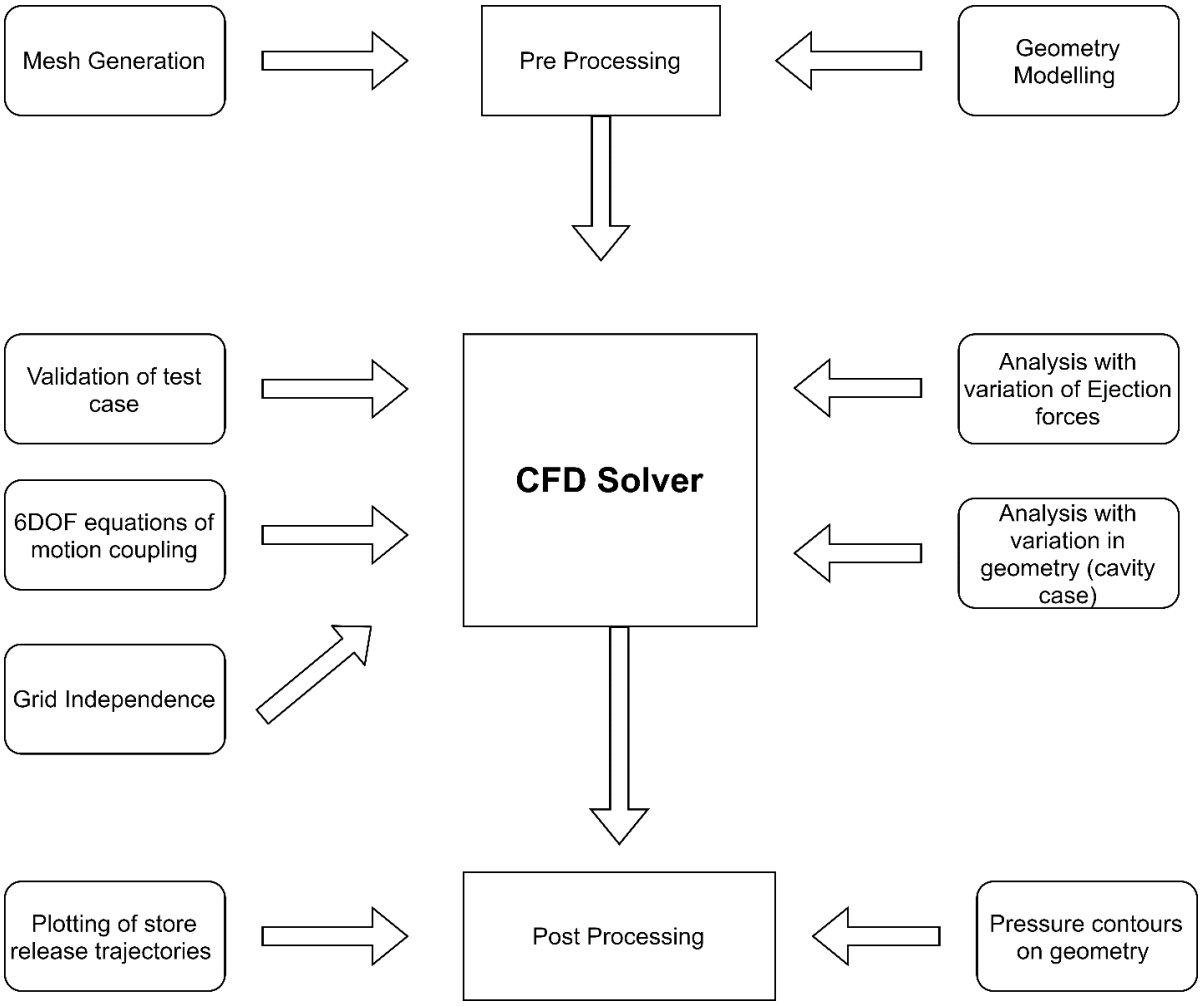

Figure 20: Numerical Methodology [41]

3.10. Technology of coupling solve

Figure 21 shows the flow chart for the coupling solutions.

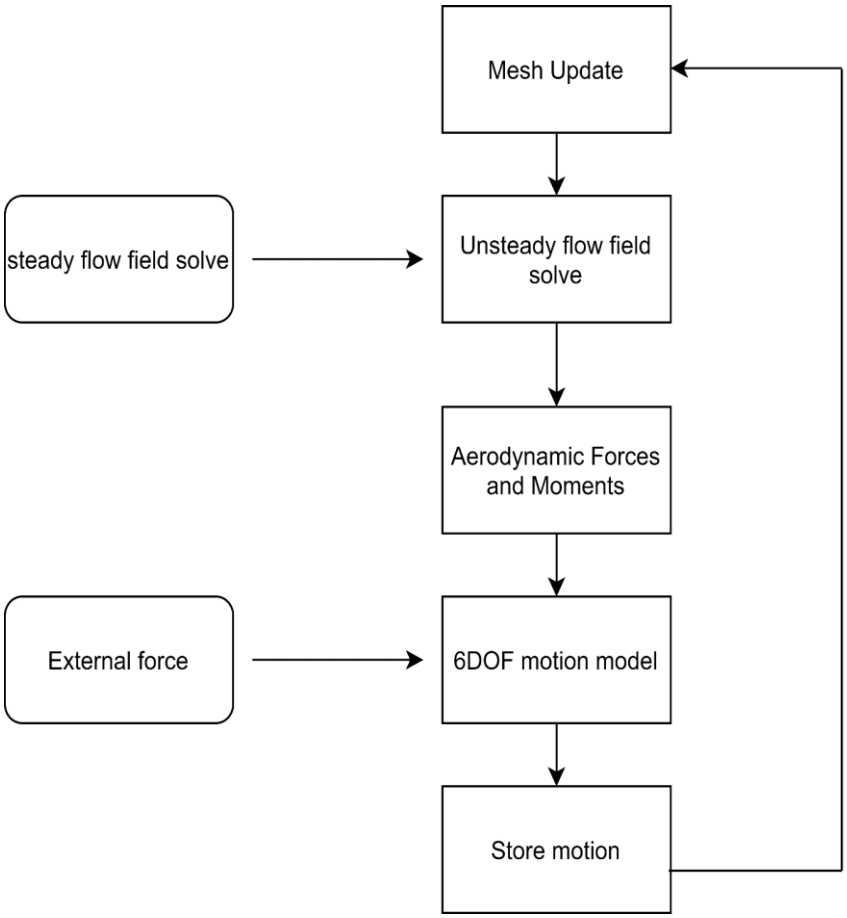

Figure 21: Flow Chart of Coupling Solve [41]

3.11. Defining and compiling UDF

3.11.1. User-defined function (UDF)

ANSYS ® FLUENT dynamically loads C-written UDF code. It has many uses, like initializing solutions, modifying boundaries, and defining material properties. These comprise the mass, moment, and products of inertia, as well as the characteristics of moment and moment properties of external forces. If desired, the aspects of an item composed of numerous zones can shift over time. The pressures and moments exerted by an external load can be defined using global or body coordinates. In addition, we can define individualized transformation matrices by utilizing the DEFINE SDOF PROPERTIES function of the UDF. In our scenario involving the store separation, the UDF designated “delta missile” describes the case injector forces and the time-dependent moments. More specifically, the relationship between the moving object’s

current angular orientation and the external forces and moments is complex. Therefore, it is necessary for UDF must be in the compiled form before execution. The UDF can be found in Appendix A.

3.11.2. Store Mass properties/Ejector Parameters

The following table lists store/inertial mass and ejector parameters.

Table 2: Store inertial/mass and ejector parameters [41]

Mass of weapon	907 kg
Center of Mass	1417mm (aft of store nose)
Roll moment of inertial	27 kg.m2
Pitch moment of inertial	488 kg.m2
Yaw moment of inertial	488 kg.m2
Forward ejector location	1237.5mm (aft of store nose)
Aft ejector location	1746.5mm (aft of store nose)
Forward ejector force	10.7kN
Aft ejector force	42.7kN

Chapter 4

Results and Discussion

4.1. A case for validating solvers

The generic wing-pylon store is a benchmark for CFD flow solvers because of the extensive experimental data [42] available for this particular case and also predicted correctly in many cases [43, 44]. In this simulation, ANSYS ® FLUENT uses a density-based solver. The results are obtained from the transient flow field using the realizable k-ε turbulence model. We used the advection upstream splitting method (AUSM) for the convection term, whereas we used the central difference method for the viscous time. Advection upstream splitting method (AUSM) provides a more precise resolution of interface and shock incompatibilities, less susceptible to Carbuncle effects.

Using Hybrid Initialization simulation attained Convergence after around 1000 iterations. The analysis required approximately 2 seconds of Computer Cluster time per iteration to calculate the steady-state solution at a courant number of 1. The solver switches to transient as soon as the steady-state solution is complete. There are 15 iterations for each time step, with a time step size of 0.0005 seconds for transient analysis.

4.2. Trajectory Validation

It is necessary to select the 6DOF option in the dynamic mesh setup before executing the transient flow calculations where gravitational acceleration can be defined if not already defined in the boundary conditions. The 6DOF solver in ANSYS® FLUENT calculates the translational and angular motion of the object's centre of gravity using the object's forces and moments.

4.2.1. Center of gravity locations

A transient simulation at Mach-1.2 (supersonic) for 0.8 seconds Figure 22 depicts the time trajectory of the centre of gravity position compared to the experimental results. When the store separates from the wing due to the combined effects of gravity and ejector forces, it starts moving backwards, downwards, and in inside directions. After roughly t = 0.17 seconds, the inward and backward movements

start. Since ejector force and gravity dominate aerodynamic forces in the z-direction, the vertical displacement matches experimental results. There is a variation in horizontal displacement due to viscous forces. In general, linear displacements in all three directions correspond well to the overall experiment results.

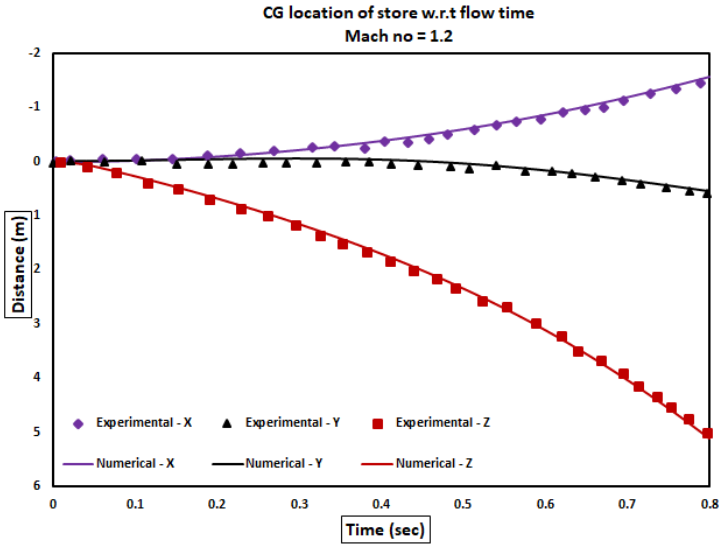

Figure 22: Trajectory of Center of Gravity Location at Mach 1.2 [35]

It was much more challenging to predict the store's orientation than the CG position, as seen in Figure 23. The degrees of yaw and pitch are in good agreement with the experiment. The store initially leans forward with its nose pointed upward in reaction to the moment that the ejectors produce. However, once free of the ejectors, the aerodynamic pitching moment causes the tendency to change in the other direction. Initially, the store will yaw outboard until roughly 0.55 seconds have passed, which will start spinning inboard. The store continues to travel outboard without stopping during the first 0.8 seconds of the separation. This trend is under-predicted by the CFD, and the curve tends to deviate from the experiments after approximately 0.3 seconds. The moment of inertia about the roll axis is significantly lower than that about the pitch and yaw axes, which makes the roll angle especially difficult to estimate.

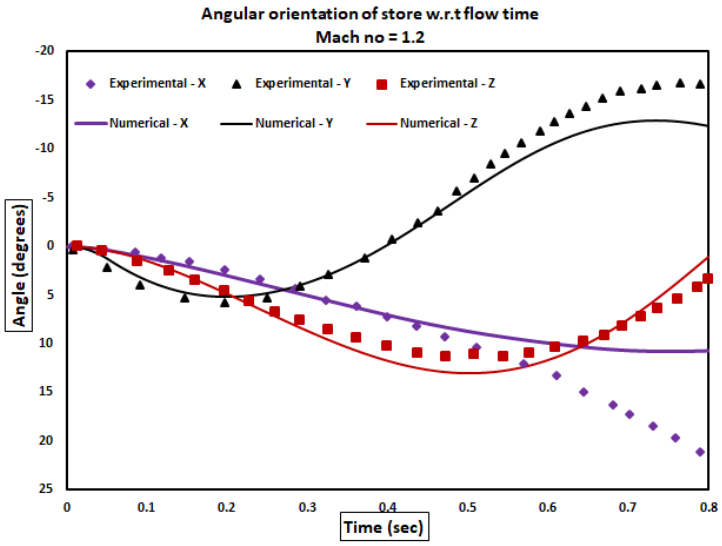

Figure 23: Trajectory of Angular Orientation of Store at Mach 1.2 [35]

4.3. Pressure contours

Figure 24 shows the pressure coefficient contours of the test case model at different time steps viewing from the side in which pitching up and right yawing movements captures.

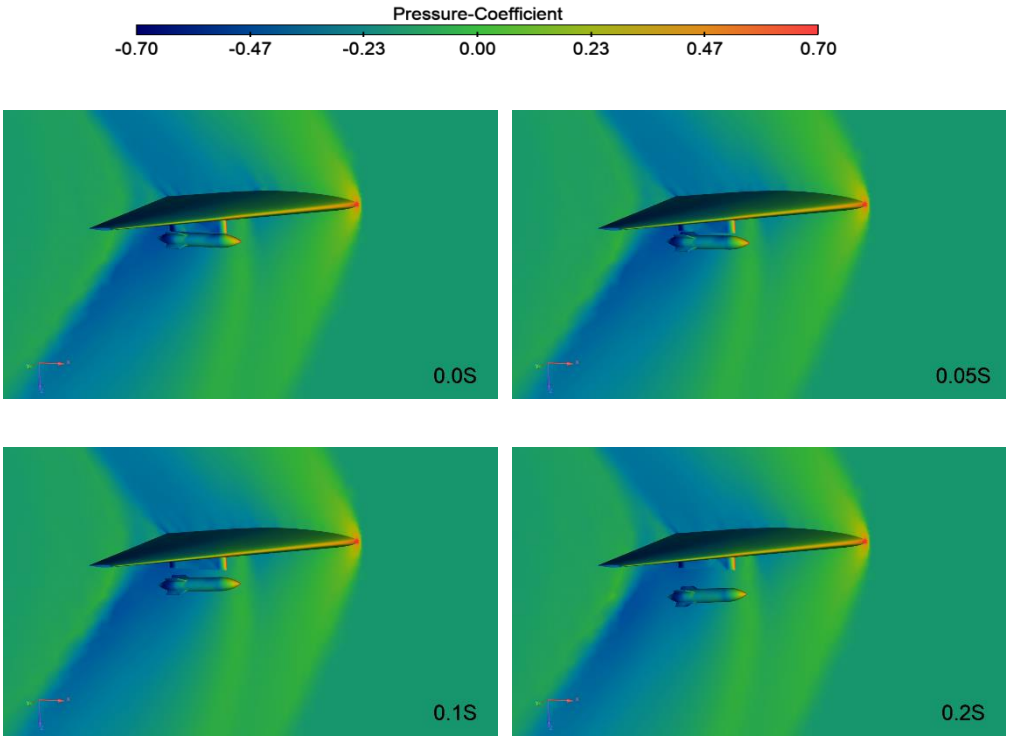

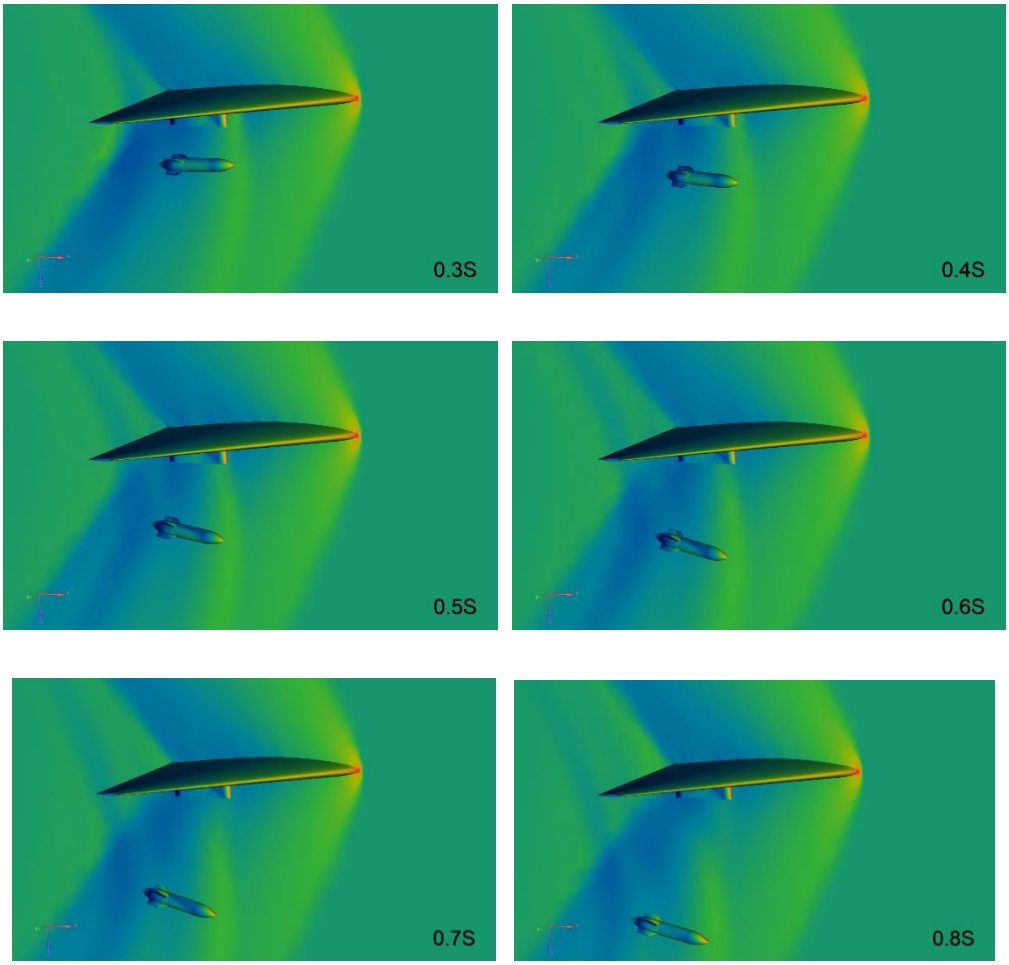

Figure 24: Pressure coefficients contours

4.4. Internal Weapon Bay Results and Analysis

For simplicity, the computational case without control devices is NCD, and rectangular and jet control devices are RCD and JCD.

4.4.1. Influence of design modification and control devices on the flow field of weapon

4.4.1.1. NCD – Original Weapon

The pressure distribution contours in the symmetry plane (XYZ) at ten different times during the separation process are in Figure 25. There is a robust shear layer located below the internal weapon bay in the NCD – Original case. The weapon passes through the shear layer and experiences a significant aerodynamic force modification. It generates high pressure on the lower surface of the weapon's head, causing the pilot to rise during the separation process. Due to the absence of a control device, the pressure

at the rear of the cavity is higher than the pressure at the front, causing the weapon to lift higher, which is risky since the store might move up and strike an aircraft component.

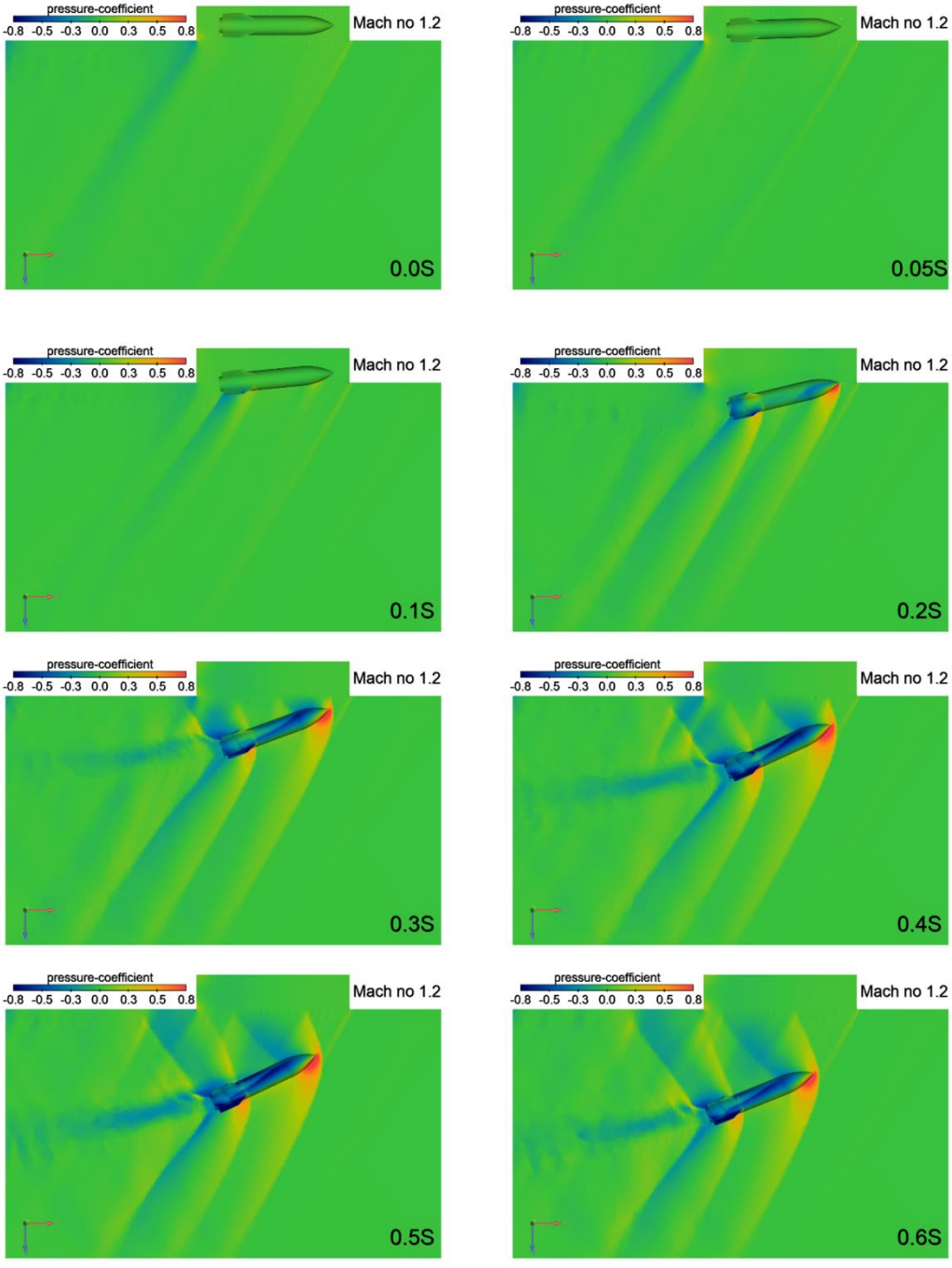

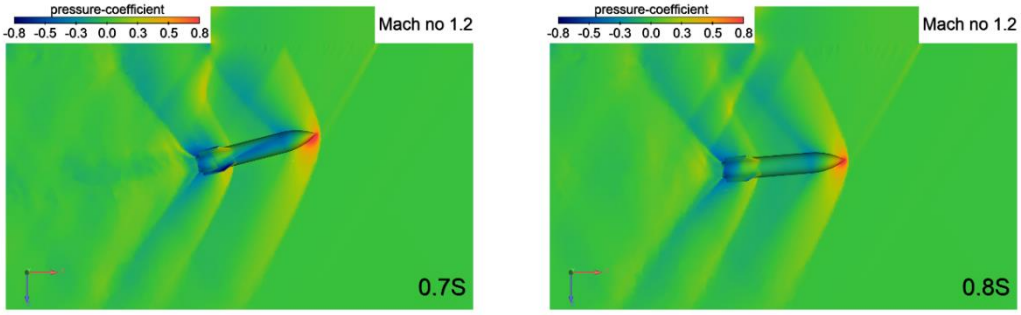

Figure 25: Pressure distribution contours NCD – Original

4.4.1.2. NCD – Modified Weapon

"Boattail" refers to the decreasing section at the weapon's end. When a body has a base that is "squared off," the boattail is added to reduce the drag that the body generates. Because of the large base area, the latter feature has a relatively large base pressure and, consequently, a high drag value. By "boat tailing" the rear part of the body, the bottom region of the body decreases, thereby decreasing the base drag. Also, after the numerical computation (t = 0.8s), Figure 26 shows that the pitch angles varied from 20 degrees to -10 degrees with boat tailing and from 26 degrees to 5 degrees without boat tailing, indicating that boat tailing helps reduce pitch angle.

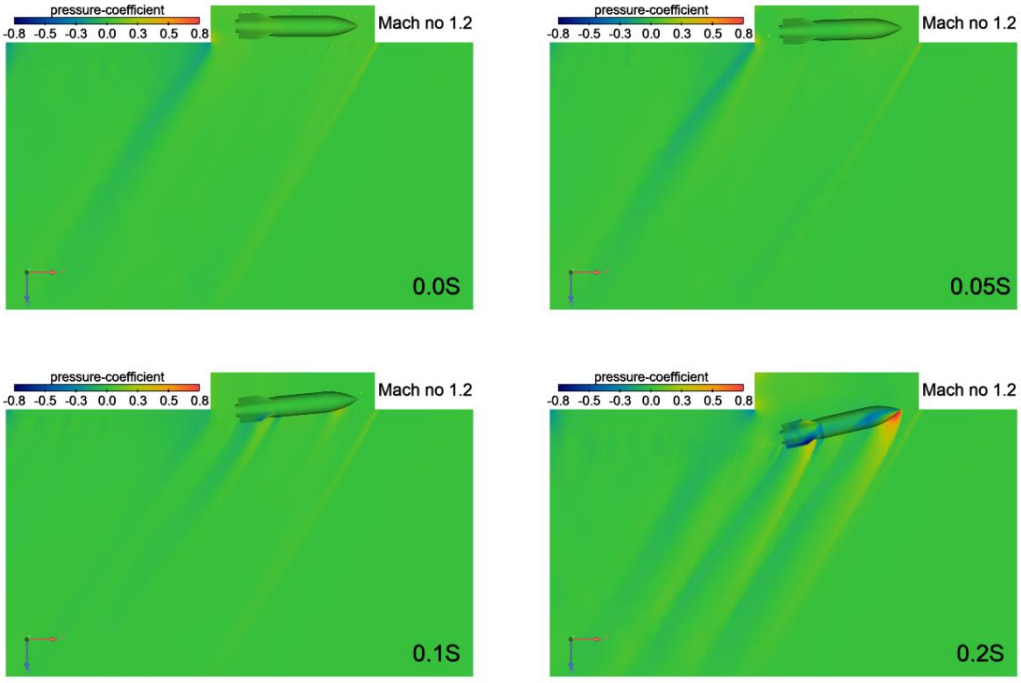

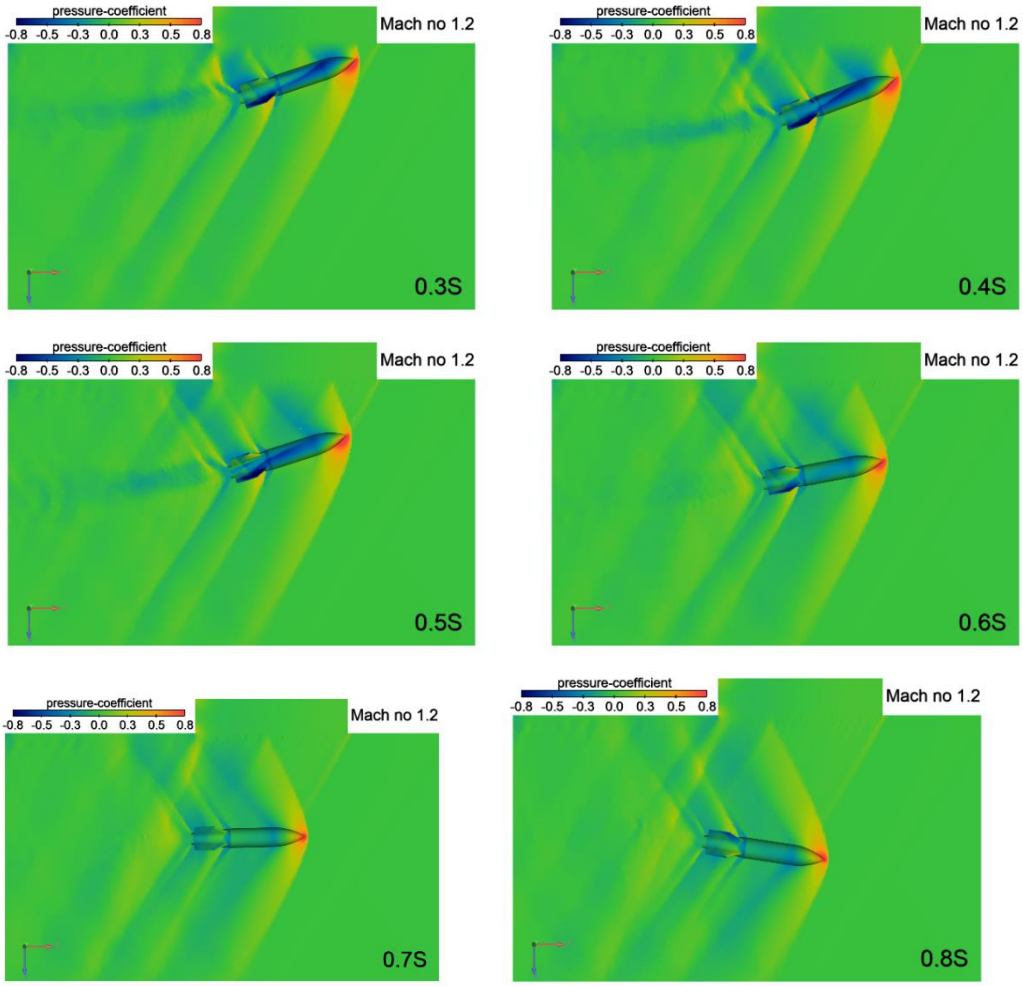

Figure 26: Pressure distribution contours NCD – Modified

4.4.1.3. NCD – Drum type

Figure 27 depicts the pressure distribution on a "drum type" weapon model. The tail is a cylindrical shroud ring supported from the after body on four symmetrical fins. The shroud ring raises the shear layer and blocks airflow entering the cavity's back portion. In this example, the shear layer underneath the weapon bay widens, allowing the weapon to travel through it smoothly. The cylindrical shroud ring postpones the shear layer's change in velocity, reducing the weapon's pitching moment during the separation procedure and enhancing the store's attitude. Furthermore, if the shroud of the drum-type tail slightly increased in diameter, it is believed that still less pitch moment would result.

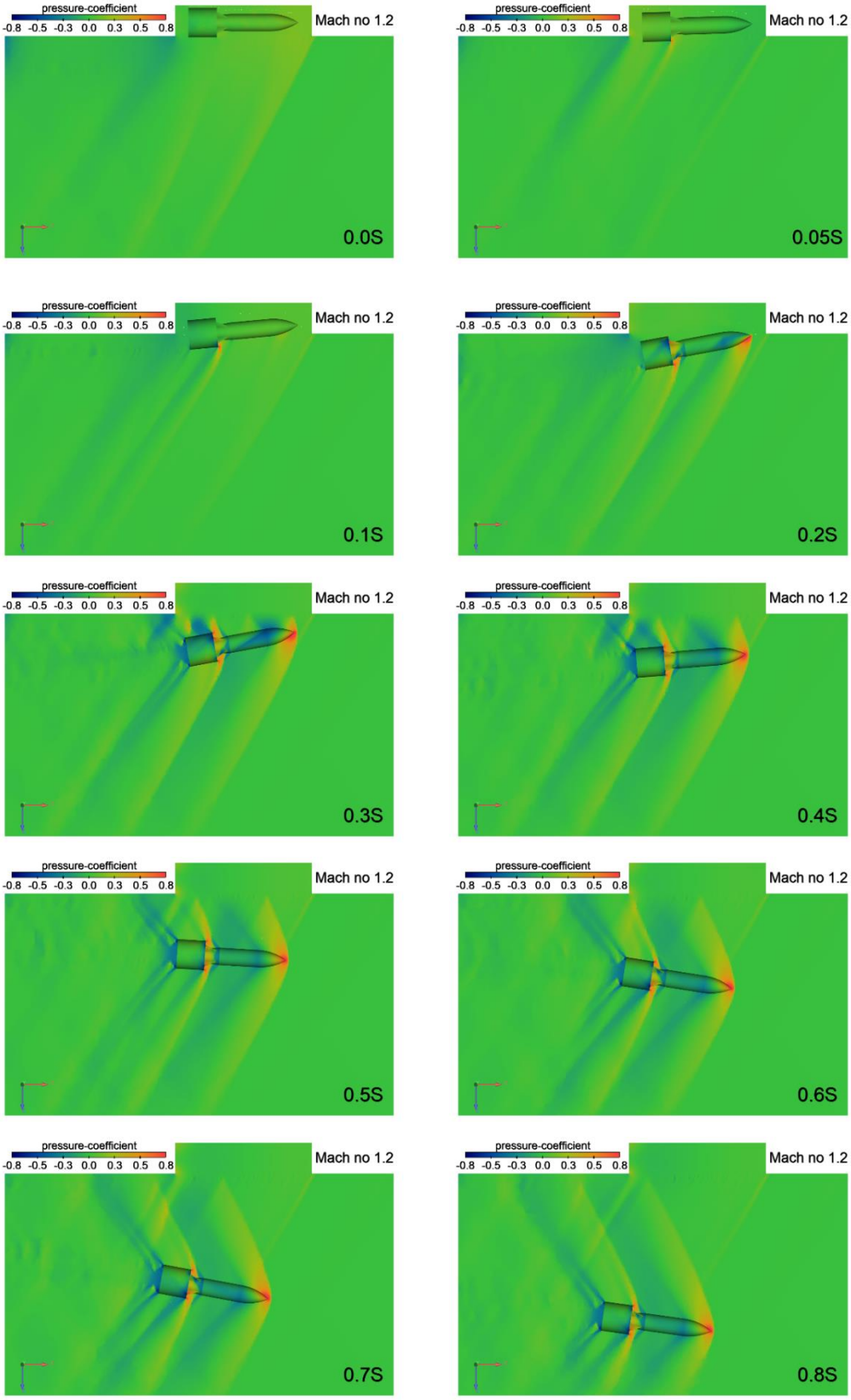

Figure 27: Pressure distribution contours NCD – Drum type

4.4.1.4. RCD – Original Weapon

Rectangular control devices (RCDs) are shown in Figure 28, illustrating the flow field characteristics of this RCD scenario. The rectangular control mechanism elevates the shear layer and decreases flux into the cavity, which drastically alters the pressure distribution within the internal weapon bay. The rectangular control device of the internal weapon bay generates a downwash shock wave with high pressure, letting the weapon pass through the shear layer without difficulty. It helps the store produce a nose-down moment of force.

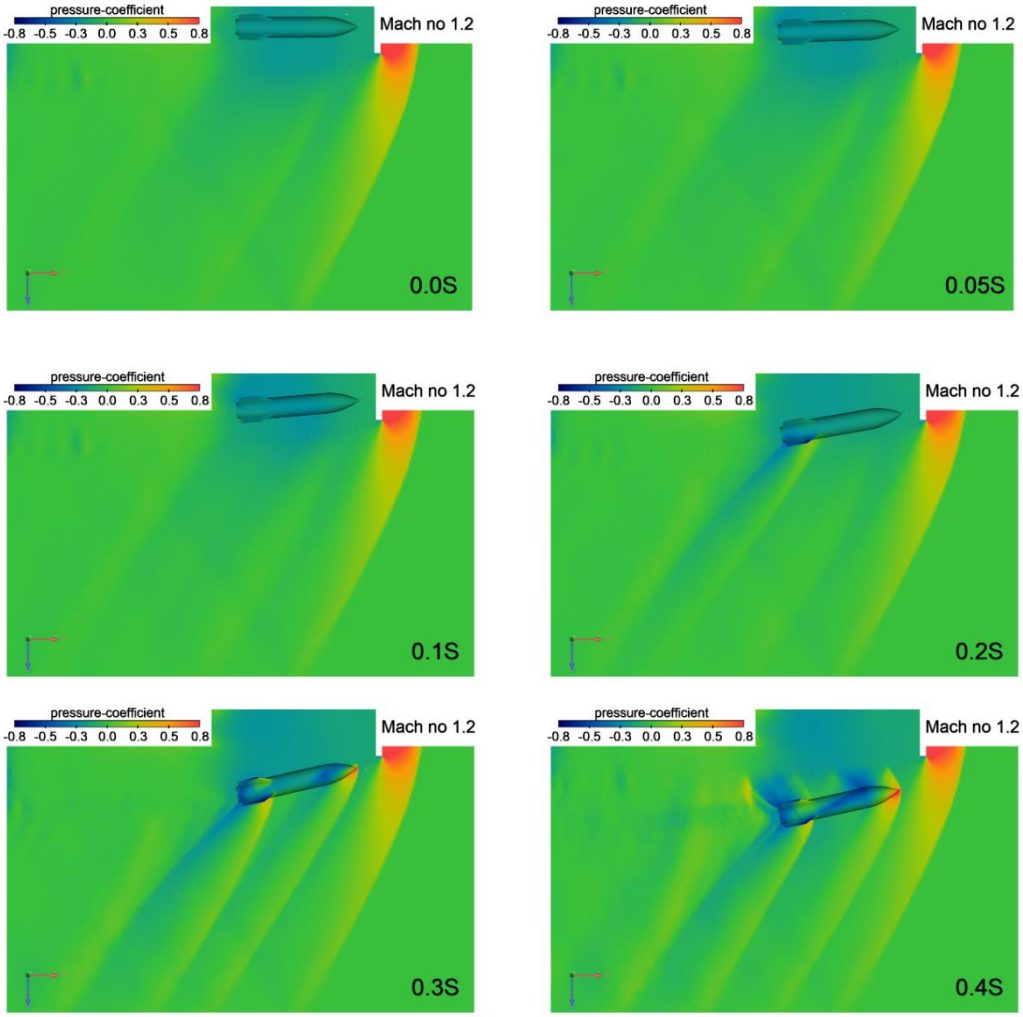

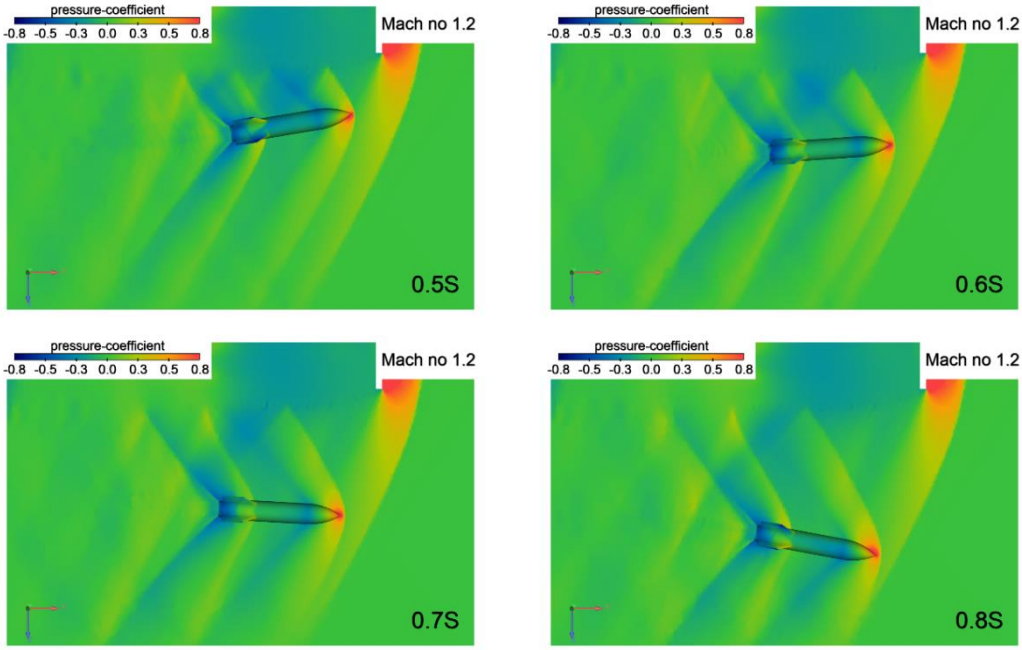

Figure 28: Pressure distribution contours RCD – Original weapon

4.4.1.5. JCD - Original Weapon

When time is more significant than zero seconds, the cavity's jet control device (JCD) becomes active. At this point, the gas from the jet will collide with the gas entering the cavity, producing shock waves. (Figure 29). The direction of the jet air was perpendicular to the jet hole; the angle between the jet and the incoming gas was θ = 90 degrees; the total gauge pressure of the jet control device was 506625Pa; the initial gauge pressure was 26497Pa. When a jet control device turns on, the shear layer beneath the bay becomes thicker. Therefore, separating the weapon to have thicker shear layers with more gradual velocity gradients is beneficial. In addition, when the jet's high pressure encounters the incoming gas, a shock wave is produced directly beneath the jet control device, and the shear layer of the bay expands. When the weapon separates through the shear layer, the lift force is significantly reduced compared to the NCD – Original case, which helps to facilitate the weapon's movement toward the state of separation.

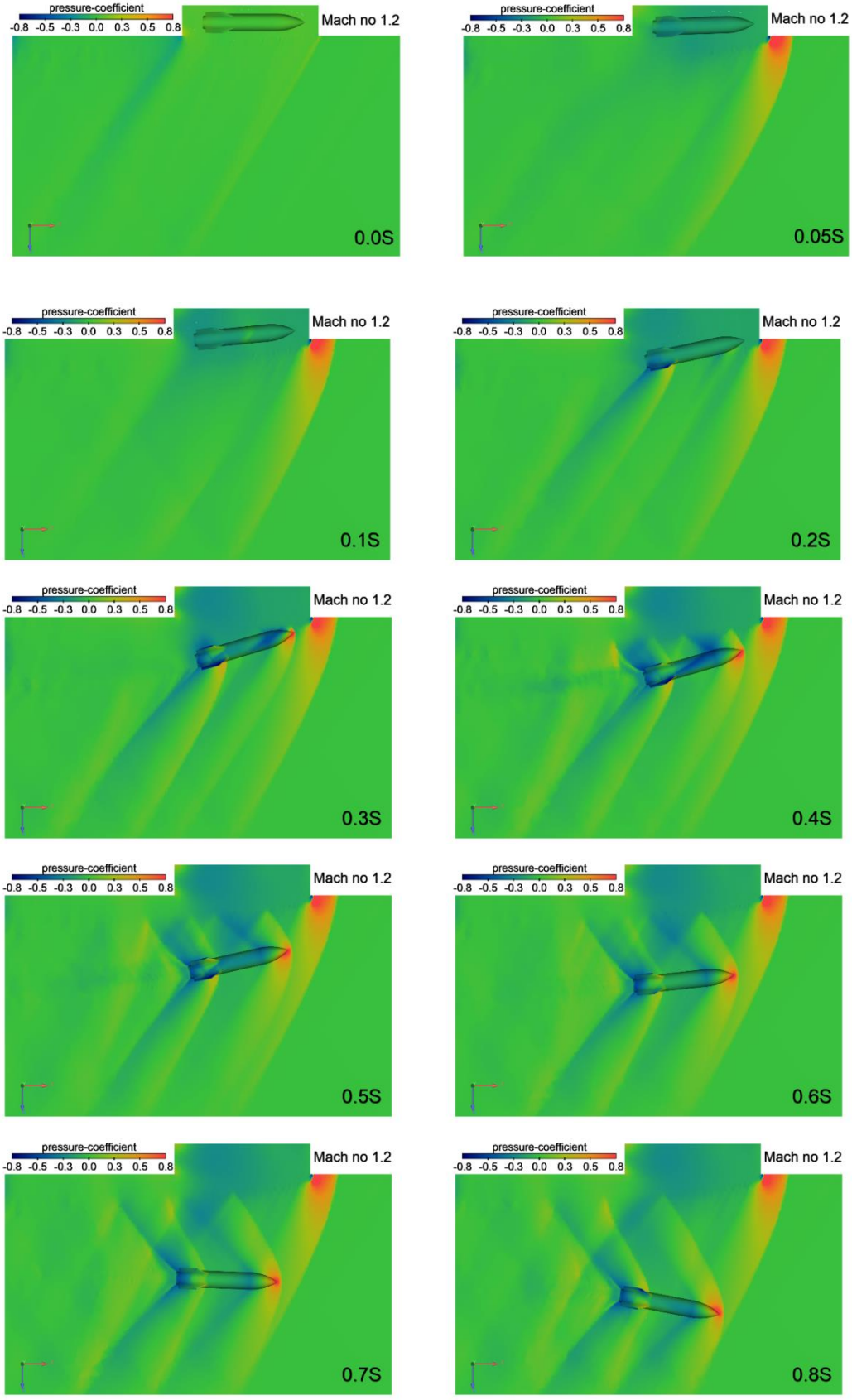

Figure 29: Pressure distribution contours JCD – Original weapon

4.4.2. Effect of design modification and control devices on the trajectory of the weapon

Figure 30 depicts the X-axis position of the weapon's centre of gravity (CG). When time is less than 0.20 seconds, the missile has a nearly identical displacement in the X direction. However, when t is more significant than 0.20 seconds, the expulsion of the weapon in the X-direction increases quickly for both the original and modified cases of the NCD. Still, it rises slowly for both instances of the flow-controlled device. The fundamental cause of weapons drifting rearward is the unavailability of the control device, which leads to a greater angle of attack of weapon drag acting on it. However, it does not raise any safety problems concerning the separation of the stores.

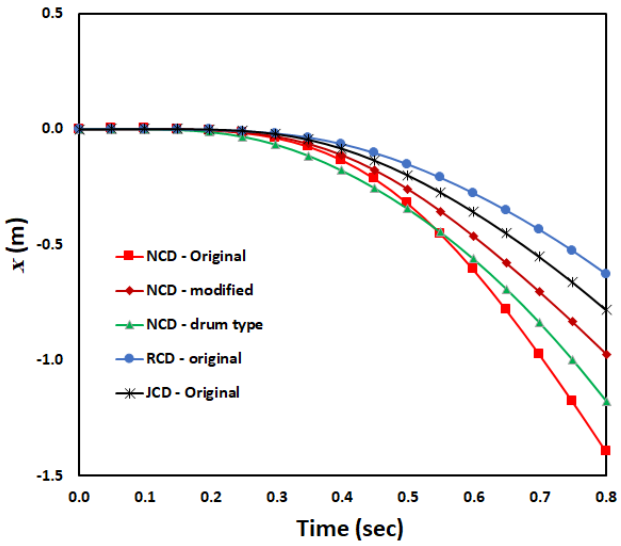

Figure 30: Evolution of centre of gravity of the missile in X-Direction

Figure 31 displays the weapon's CG position on the Z-axis. When t is less than 0.4s, all five cases have separations near one another. For the NCD-Original, the slightest movement occurs along Z-direction; this is so because the pressure in the back of the bay is higher than the front, and the weapon angle of attack increases rapidly. The maximum missile displacement, as calculated numerically (t = 0.8s), is 4.8 m for the NCD - drum type case, which is 1.6 times greater than the original case.

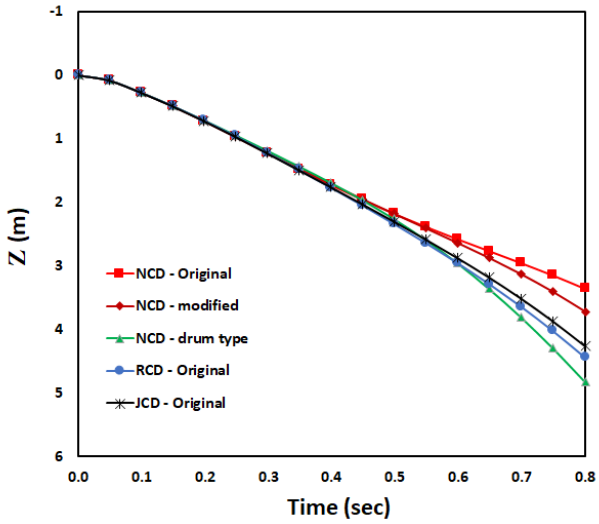

Figure 31: Evolution of centre of gravity of the missile in Z-Direction

Figure 32 illustrates the global coordinate system's pitch angle variation. In the separation process, all the cases show different trends in pitch angle. For the weapon in NCD – Original case, a strong aerodynamic force generates high pressure on the lower surface, and a strong shear layer at the rear of the cavity makes the missile pitch angle high. This intense pitch motion may cause it to collide with the weapon bay at a high angle of attack. In NCD – The modified case, the base area reduces by boat tailing: As a result, the missile's motion as it pitches is not extremely serious, and the pitching angle of the store varies from twenty degrees to minus ten degrees. The graph also shows that the jet and rectangular control devices have almost the same potential to nose down the store, but the gentlest and stable pitching behaviour showed NCD – drum-type case ranging from 9° to -9.5°.

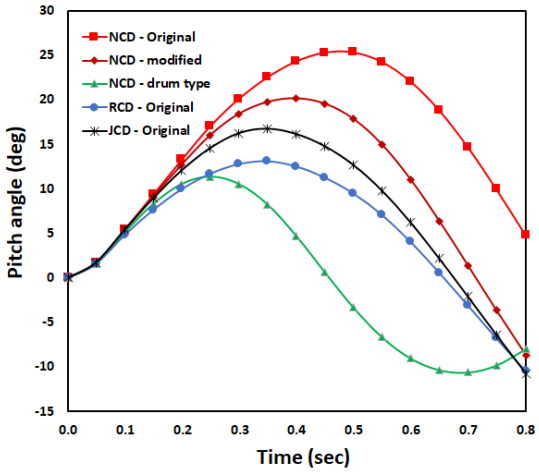

Figure 32: Time-varying angular orientation of Y - axis

Figure 33 illustrates the pitching moment coefficient (**C**M*y*) of the weapon. Under the action of high pressure in the rear of the bay and incoming flow Figure 4.4, the store suffered a big pitching moment. Rapid growth in CMy - NCD Original is observed, with a maximum value attained at a separation time of 0.55 s. For times more significant than 0.55s, **C**M*y* – NCD Original decreases as pressure behind the missile drops and pressure above the weapon's head rises. The **C**M*y* – NCD modified also increases quickly at first and stays around 1.3, then decreases until it reaches 0.35, which improves pitch angle. The pitching moment coefficient **C**M*y* rises first and remains constant until the simulation time ends in the RCD and JCD cases. In the case of the NCD – drum, the pitching moment coefficient (**C**M*y*) does not change significantly and gives a minimum value of around 0.5 at t = 0.52 s. The store's attitude is stable, and its nose will be downward quickly—figure 4.6: When t > 0.52 s, the **C**M*y* – NCD drum type increases. Since the **C**M*y* – NCD drum type case pitching is not intense, the missile attitude will remain gentle.

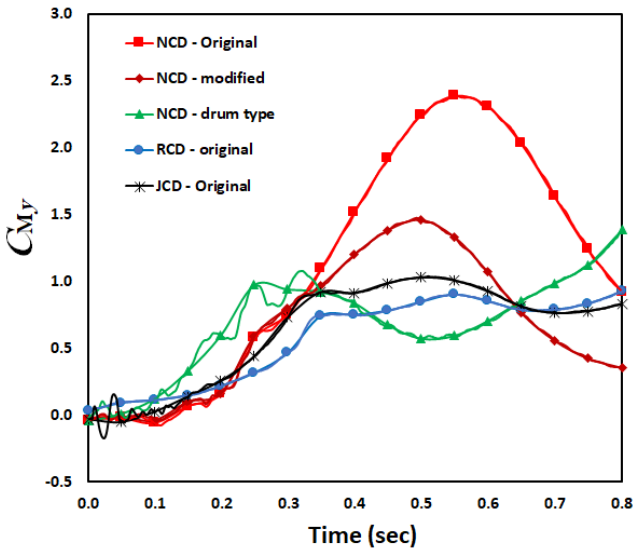

Figure 33: Pitching moment coefficient

4.5. Separation process of missile

Figure 34 shows the weapon's orientation. Nine visual moments show weapon separation. NCD – drum-type weapon case shows how quickly the store leaves the bay. At t=0.8s, the missile's z-direction distance is the greatest. Flow control devices (RCD

and JCD) have a gentle pitch angle and weapon attitude. Compared to the NCD-Original weapon case, weapon separation is safe and secure.

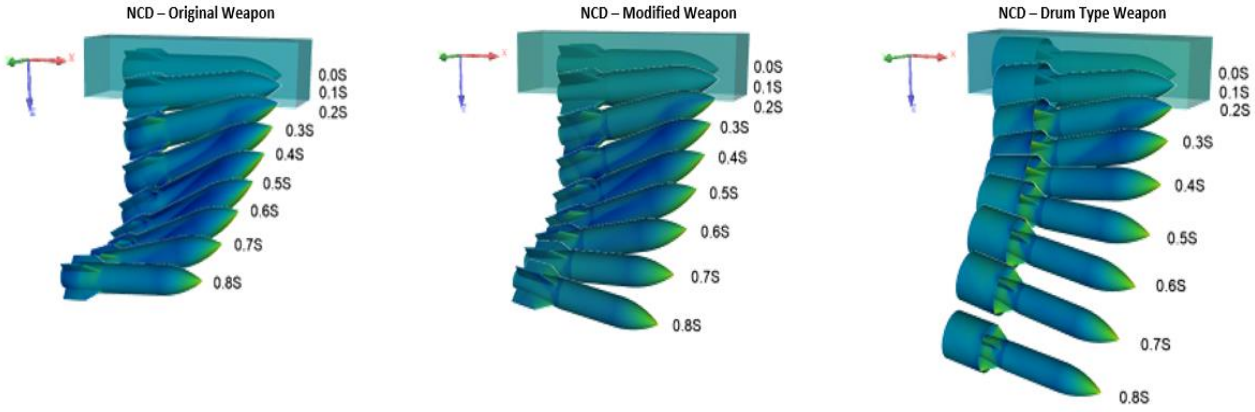

(a)

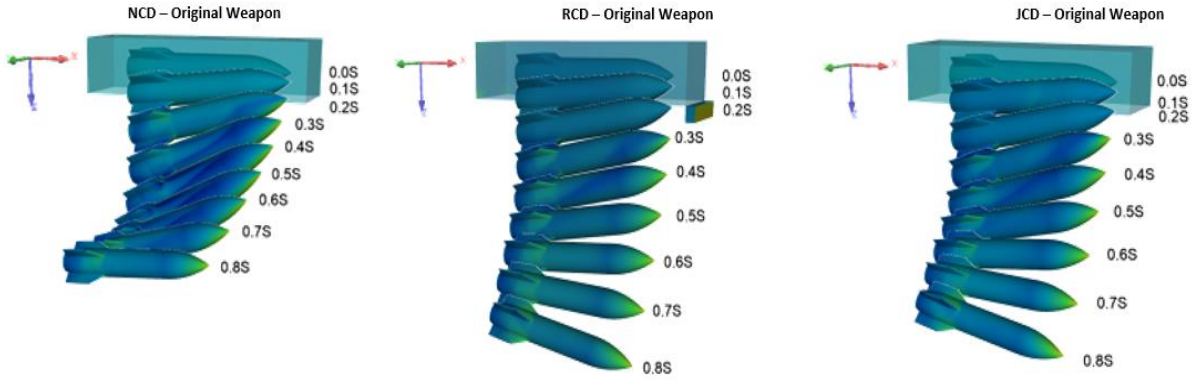

(b)

Figure 34: Separation process of the store: (a) influence of design modification (b) with flow control devices

Chapter 5

Conclusion and Future work

5.1. Conclusion

The current study analyzed the store separation trajectory using N-S equations, 6DOF rigid-body equations, and overset dynamic mesh technology. During the separation process, the weapon slides backward, below, and inboard, and the results showed an excellent fit with experimental data. After validation, we analyzed the Influence of design modification and control devices on the flow characteristics of the store from the weapon bay under the following five scenarios: Free separation, modified design, drum type modification, and flow control devices (rectangular and jet). The findings are summarized as follows based on our numerical results.

- In the NCD-Original case, pressure in the back of the cavity is higher than in the front, leading the weapon to lift upward, which is risky because the store could rise and hit an aircraft part.
- After adding the boattail structure, the drag and pitch angle decreases compared to the NCD-Original case. The CMy - NCD modified case goes up at first, staying around 1.3, then falls until it reaches 0.35, reducing pitch angle and advantageous.
- In the drum-type case, the cylindrical ring prevents airflow into the back portion of the cavity, which helps to reduce its pitch angle. At the end of the numerical simulation(t=0.8s), the missile covers a significant distance in the z-direction compared to all other cases. Furthermore, if the shroud of the drum-type tail slightly increased in diameter, it is believed that still less pitch angle would result.
- The Rectangle and Jet control devices (RCD & JCD) placed at the cavity's leading edge may alter the shear layer, enhance the flow field's dynamics, and let the weapon quickly pass through the shear layer when released from the bay. It can also improve the pitch angle to be gentle and stable and ensure the safe separation of weapons.

- Our results suggest that instead of mounting control devices on the cavity front that cause drag, optimisation in weapon design can achieve better flow field aerodynamic and trajectory parameters.

5.2. Future work

- Restrain the missile's ejection mechanism.
- Machine learning-based clustering of weapon-separation trajectories.
- Maneuvering aircraft effects on weapon trajectories.

Appendix A

UDF CODE

```
/*****************************************************
SDOF property compiled UDF with external forces/moments
*****************************************************/

#include "udf.h"

DEFINE_SDOF_PROPERTIES(delta_missile,  prop,  dt,  time,
dtime) {
    prop[SDOF_MASS] = 907.185;
    prop[SDOF_IXX] = 27.116;
    prop[SDOF_IYY] = 488.094;
    prop[SDOF_IZZ] = 488.094;
    /* add injector forces, moments */
    {
      register real dfront = fabs(DT_CG(dt)[2] - (0.179832
* DT_THETA(dt)[1]));
      register real dback = fabs(DT_CG(dt)[2] + (0.329184
* DT_THETA(dt)[1]));
      if (dfront <= 0.100584) {
        prop[SDOF_LOAD_F_Z] = 10676.0;
        prop[SDOF_LOAD_M_Y] = -1920.0;
      }
      if (dback <= 0.100584) {
        prop[SDOF_LOAD_F_Z] += 42703.0;
        prop[SDOF_LOAD_M_Y] += 14057.0;
      }
    }
    printf("missile : updated6DOF properties”);
    }
```

References

[1] A. Cenko, P. Richardson, M. Talbot, S. Loezos, D. Chaddock, and A. Piranian, "Integrated t&e approach to store separation-dim past, exciting future." pp. 541-551.

[2] J. V. GARCÍA. "Top guns of World War I," 13 September, 2022; https://www.nationalgeographic.co.uk/history-and-civilisation/2018/11/top-guns-of-world-war-i.

[3] M. CFD. "How to Improve the Aerodynamic Performance of Aircraft in the Industry using CFD Simulation?," 13 October, 2022; https://www.mr-cfd.com/industries/aerodynamic-and-aerospace-engineering/.

[4] A. Cenko, "Store Separation Lessons Learned During the Last 30 Years."

[5] M. Bamber, "Two methods of obtaining aircraft trajectories from wind tunnel investigations," *AERO Report*, vol. 970, 1960.

[6] C. L. Bore, "Integrated design of fighters with stores for best airforce value," *Progress in Aerospace Sciences*, vol. 33, no. 11, pp. 709-730, 1998/04/14/, 1998.

[7] T. Buchanan, and W. Crosby, *Captive Trajectory System Test Planning Information for AEDC Supersonic Wind Tunnel (A) and Hypersonic Wind Tunnels (B) and (C)*, ARNOLD ENGINEERING DEVELOPMENT CENTER ARNOLD AFB TN, 1983.

[8] D. Hill Jr, J. Best, and R. Tolbert, *Comparison of Store Trajectory and Aerodynamic Loads, and Model Flow-Field Characteristics Obtained in the AEDC PWT/4T and VFK/A Wind Tunnels at Mach Number 1.63*, ARO INC ARNOLD AFS TN, 1979.

[9] M. Madson, S. Moyer, and A. Cenko, "TranAir computations of the flow about a generic wing/pylon/finned-store configuration." p. 155.

[10] A. Cenko, J. Lee, E. Getson, E. Hallberg, B. Jolly, and W. Sickles, "IHAAA applications to reducing store separation flight testing," *2007 US Air Force T&E Days*, p. 1653, 2007.

[11] M. Madson, and M. Talbot, "F-16/generic store carriage load predictions at transonic Mach numbers using TranAir." p. 2454.

[12] A. Cenko, and M. Lutton, "ACFD Applications to store separation—status report," *The Aeronautical Journal*, vol. 104, no. 1040, pp. 459-466, 2000.

[13] A. Cenko, R. Meyer, and F. Tessitore, "Further development of the influence function method for store aerodynamic analysis," *Journal of Aircraft*, vol. 23, no. 8, pp. 656-661, 1986.

[14] A. Cenko, "One CFD calculation to end point flight testing:(Has CFD finally replaced the wind tunnel?)," *The Aeronautical Journal*, vol. 110, no. 1109, pp. 439-446, 2006.

[15] A. Cenko, D. Grove, and J. Lee, "'IHAAA Applications to Store Separation," *ICAS paper P*, vol. 2, 2006.

[16] R. L. Stallings Jr, “Store separation from cavities at supersonic flight speeds,” *Journal of Spacecraft and Rockets,* vol. 20, no. 2, pp. 129-132, 1983.

[17] O. Baysal, K. Fouladi, R. Leung, and J. Sheftic, “Interference flows past cylinder-fin-sting-cavity assemblies,” *Journal of aircraft,* vol. 29, no. 2, pp. 194-202, 1992.

[18] L. N. Cattafesta III, Q. Song, D. R. Williams, C. W. Rowley, and F. S. Alvi, “Active control of flow-induced cavity oscillations,” *Progress in Aerospace Sciences,* vol. 44, no. 7-8, pp. 479-502, 2008.

[19] A. J. Saddington, V. Thangamani, and K. Knowles, “Comparison of passive flow control methods for a cavity in transonic flow,” *Journal of Aircraft,* vol. 53, no. 5, pp. 1439-1447, 2016.

[20] W. Jifei, L. Xinfu, and F. Zhaolin, “Flow control method to improve cavity flow and store separation characteristics,” *Acta aeronautica et Astronautica sinica,* vol. 30, no. 10, pp. 1840-1845, 2009.

[21] S. Perng, and D. Dolling, “Suppression of pressure oscillations in high-Mach-number, turbulent, cavity flow,” *Journal of Aircraft,* vol. 38, no. 2, pp. 248-256, 2001.

[22] N. Vikramaditya, and J. Kurian, “Effect of aft wall slope on cavity pressure oscillations in supersonic flows,” *The Aeronautical Journal,* vol. 113, no. 1143, pp. 291-300, 2009.

[23] C. Lada, and K. Kontis, “Experimental studies of open cavity configurations at transonic speeds with flow control,” *Journal of Aircraft,* vol. 48, no. 2, pp. 719-724, 2011.

[24] M. Martinez, G. M. Di Cicca, M. Iovieno, and M. Onorato, “Control of cavity flow oscillations by high frequency forcing,” *Journal of fluids engineering,* vol. 134, no. 5, 2012.

[25] N. Vikramaditya, and J. Kurian, “Pressure oscillations from cavities with ramp,” *AIAA journal,* vol. 47, no. 12, pp. 2974-2984, 2009.

[26] S. Lawson, and G. Barakos, “Assessment of passive flow control for transonic cavity flow using detached-eddy simulation,” *Journal of aircraft,* vol. 46, no. 3, pp. 1009-1029, 2009.

[27] A. D. Vakili, and C. Gauthier, “Control of cavity flow by upstream mass-injection,” *Journal of Aircraft,* vol. 31, no. 1, pp. 169-174, 1994.

[28] M. Davis, P. Yagle, B. Smith, K. Chankaya, and R. Johnson, "Store trajectory response to unsteady weapons bay flowfields." p. 547.

[29] F. Xue, X. Jin, Y. C. Wang, and Y. N. Yang, “Wind tunnel test technique on high speed weapon delivery from internal weapons bay,” *Acta Aeronautica et Astronautica Sinica,* pp. 59-65 2017.

[30] D. Sahoo, A. Annaswamy, and F. Alvi, "Microjets-based active control of store trajectory in a supersonic cavity using a low-order model." p. 3097.

[31] V. Shalaev, A. Fedorov, and N. Malmuth, “Dynamics of slender bodies separating from rectangular cavities,” *AIAA journal*, vol. 40, no. 3, pp. 517-525, 2002.

[32] D. Sahoo, A. Annaswamy, and F. Alvi, “Active store trajectory control in supersonic cavities using microjets and low-order modeling,” *AIAA journal*, vol. 45, no. 3, pp. 516-531, 2007.

[33] W. Bower, V. Kibens, A. Cary, F. Alvi, G. Raman, A. Annaswamy, and N. Malmuth, "High-frequency excitation active flow control for high-speed weapon release (HIFEX)." p. 2513.

[34] A. Ali. "CFD Workflow Guide: How to Set Up a Fluid Dynamics Analysis," September 8, 2022; https://www.simscale.com/blog/cfd-workflow-quick-guide/.

[35] E. R. Heim, *CFD wing/pylon/finned store mutual interference wind tunnel experiment*: Arnold Engineering Development Center, Air Force Systems Command, United …, 1991.

[36] R. Kannan, and Z. Wang, “Overset adaptive Cartesian/prism grid method for stationary and moving-boundary flow problems,” *AIAA journal*, vol. 45, no. 7, pp. 1774-1779, 2007.

[37] A. Inc, "Ansys User Manual," ANSYS Inc.

[38] C. NINJA. "Ansys Fluent Tutorial | Overset Mesh," 13 October, 2022; https://cfd.ninja/ansys-fluent/ansys-fluent-tutorial-overset-mesh/.

[39] A. Khaware, A. Shivanandham, V. K. Gupta, S. Ramakrishnan, M. Azab, and T. Scheidegger, "Numerical simulation of store separation trajectories for EGLIN test case using overset mesh." p. 1272.

[40] A. Inc, "Ansys Theory Manual," ANSYS Inc.

[41] M. Sheharyar, E. Uddin, Z. Ali, Q. Zaheer, and A. Mubashar, “Simulation of a Standard Store Separated from Generic Wing,” *Journal of Applied Fluid Mechanics*, vol. 11, no. 6, pp. 1579-1589, 2018.

[42] J. H. Fox, *Generic wing, pylon, and moving finned store*, SVERDRUP TECHNOLOGY INC ARNOLD AFS TN, 2000.

[43] L. E. Lijewski, and N. E. Suhs, “Time-accurate computational fluid dynamics approach to transonic store separation trajectory prediction,” *Journal of Aircraft*, vol. 31, no. 4, pp. 886-891, 1994.

[44] L. Hall, C. Mitchell, V. Parthasarathy, L. Hall, C. Mitchell, and V. Parthasarathy, "An unsteady simulation technique for missile guidance and control applications." p. 636.